nature cell biology

Endothelial podosome rosettes regulate vascular branching in tumour angiogenesis

Giorgio Seano[1,2,3,9], Giulia Chiaverina[1,2], Paolo Armando Gagliardi[1,2], Laura di Blasio[1,2], Alberto Puliafito[1,2], Claire Bouvard[4,8], Roberto Sessa[1,2,8], Guido Tarone[5], Lydia Sorokin[6], Dominique Helley[7], Rakesh K. Jain[3], Guido Serini[1,2], Federico Bussolino[1,2] and Luca Primo[1,2,9]

The mechanism by which angiogenic endothelial cells break the physical barrier of the vascular basement membrane and consequently sprout to form new vessels in mature tissues is unclear. Here, we show that the angiogenic endothelium is characterized by the presence of functional podosome rosettes. These extracellular-matrix-degrading and adhesive structures are precursors of *de novo* branching points and represent a key feature in the formation of new blood vessels. VEGF-A stimulation induces the formation of endothelial podosome rosettes by upregulating integrin $\alpha_6\beta_1$. In contrast, the binding of $\alpha_6\beta_1$ integrin to the laminin of the vascular basement membrane impairs the formation of podosome rosettes by restricting $\alpha_6\beta_1$ integrin to focal adhesions and hampering its translocation to podosomes. Using an *ex vivo* sprouting angiogenesis assay, transgenic and knockout mouse models and human tumour sample analysis, we provide evidence that endothelial podosome rosettes control blood vessel branching and are critical regulators of pathological angiogenesis.

Angiogenesis, the development of new vessels from pre-existing ones, plays a critical role in cancer progression. Endothelial cells (ECs), which lead this process, need to overcome several mechanisms attempting to keep the vascular network quiescent. To sprout and form new vessels, the first barrier that ECs have to cross is the vascular basement membrane (vBM), composed of laminins, collagen and proteoglycans[1].

Angiogenic factors, such as the well-studied vascular endothelial growth factor[2–4] (VEGF), guide sprouting angiogenesis. When quiescent vessels sense angiogenic signals, tip ECs are stimulated to invade the underlying layer of vBM that prevents sprouting. This process requires proteolytic breakdown of selected vBM proteins that can be mediated by matrix metalloproteases (MMPs), such as membrane type-1 MMP (MT1-MMP; refs 5,6). However, the cellular mechanisms required for this process remain largely unknown.

Podosomes and invadopodia, collectively called invadosomes, are specialized cell–matrix contacts with an inherent ability to degrade extracellular matrix (ECM) in restricted areas and are typically characterized by enrichment in F-actin and cortactin[7–9]. They are considered key structures of cells that are able to cross anatomical boundaries, such as monocyte-derived cells and transformed fibroblasts[7,10]. Cultured ECs contain either isolated 1-μm-wide individual podosomes or 4–8-μm-wide ring-like clusters of podosomes, called podosome rosettes[7,11,12]. The appearance of individual podosomes and rosettes in ECs can be increased by soluble factors, such as TGF-β, or by phorbol esters[11,12]. Although endothelial podosome rosettes have been observed in TGF-β-stimulated aortic explants[11], definitive *in vivo* evidence for their existence and a functional role for such structures is still lacking.

Here, we show that endothelial rosettes are critical regulators of sprouting angiogenesis and control tumour blood vessel branching. We demonstrate how the VEGF-induced upregulation of the α_6 integrin subunit in ECs induces the formation of podosome rosettes and overcomes the vascular stabilizing and anti-angiogenic effects of the vBM laminin.

RESULTS

VEGF-A induces the assembly of podosome rosettes in ECs

Podosomes (identified by the co-localization of F-actin/cortactin at the basal side of ECs) were organized in two different

[1]Department of Oncology, University of Torino, Turin 10100, Italy. [2]Candiolo Cancer Institute-FPO, IRCCS, Candiolo 10060, Italy. [3]Edwin L. Steele Laboratory for Tumor Biology, Harvard Medical School, Massachusetts General Hospital, Boston, Massachusetts 02114, USA. [4]UMR-S 765, Université Paris Descartes, Sorbonne Paris Cité, Paris 75006, France. [5]Department of Molecular Biotechnology and Health Sciences, University of Torino, Molecular Biotechnology Center, Turin 10124, Italy. [6]Institute of Physiological Chemistry and Pathobiochemistry, Muenster University, Muenster 48149, Germany. [7]UMR-S 970, Université Paris Descartes, Sorbonne Paris Cité, Paris 75006, France. [8]Present addresses: The Scripps Research Institute, La Jolla, California 92037, USA (C.B.); Center for Eye Disease and Development, University of California, Berkeley, California 94720, USA (R.S.).
[9]Correspondence should be addressed to G.S. or L.P. (e-mail: seano@steele.mgh.harvard.edu or luca.primo@ircc.it)

Received 1 October 2013; accepted 6 August 2014; published online 14 September 2014; DOI: 10.1038/ncb3036

© 2014 Macmillan Publishers Limited. All rights reserved.

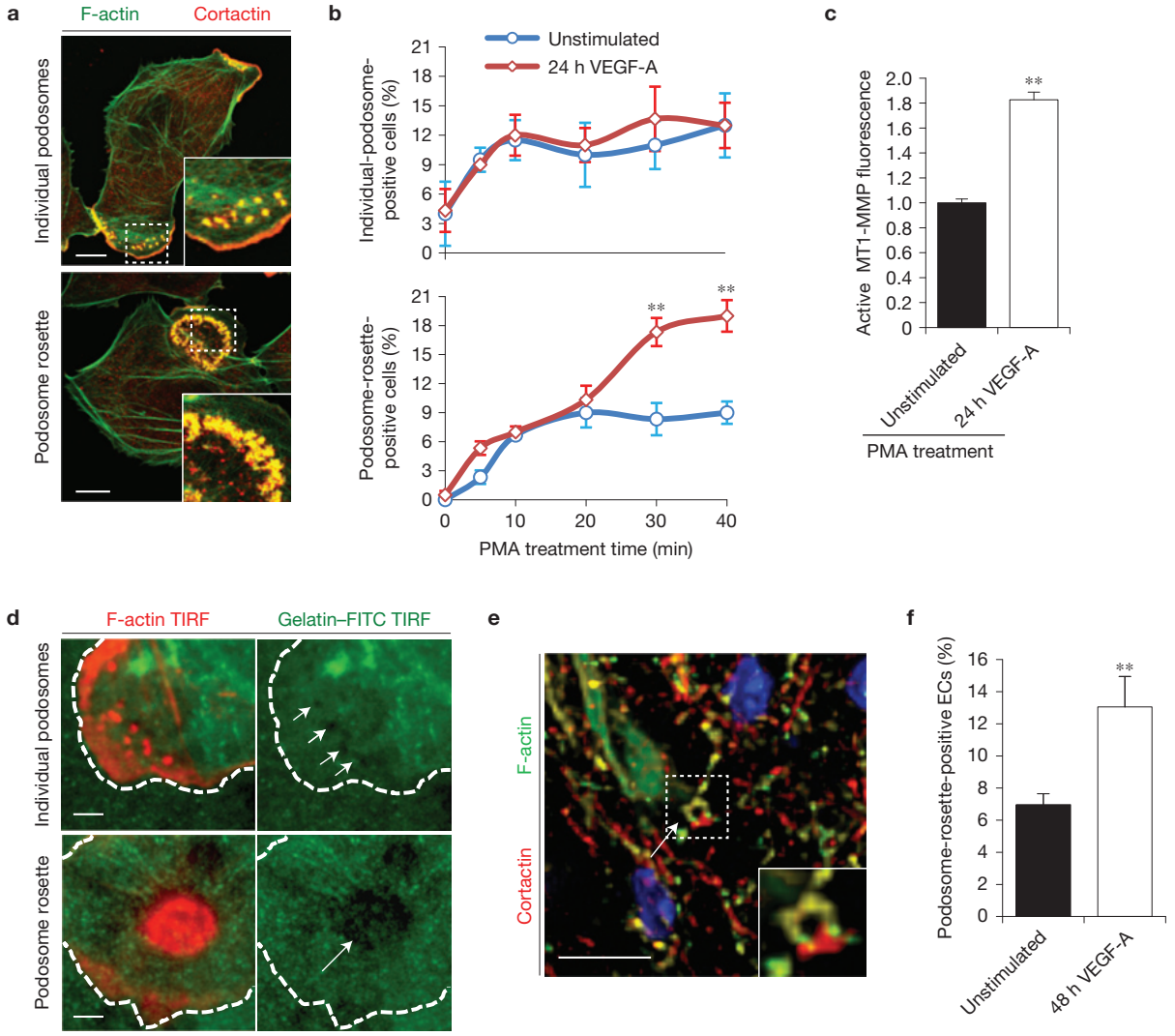

Figure 1 VEGF-A induces endothelial podosome rosettes. (**a**) Immunostained representative ECs treated with PMA for 30 min. Insets, zoom of the same micrograph. Scale bars, 10 μm. (**b**) ECs—incubated for 24 h in M199 10% FCS (unstimulated) or in M199 10% FCS plus 30 ng ml^{-1} of VEGF-A (24 h VEGF-A)—were treated for 30 min with PMA. We calculated the percentage of individual-podosome- and podosome-rosette-positive ECs, treated with PMA for the indicated times. Mean ± s.e.m. of $n=3$ independent experiments in which 250 cells were analysed per experimental point. (**c**) Cytofluorimetric analysis of the active form of MT1-MMP. ECs treated with PMA for 30 min. Normalized mean ± s.e.m. of $n=3$ independent experiments in which 9×10^4 cells were analysed per experimental point. (**d**) Gelatin degradation assay by TIRF micrographs. ECs were seeded on FITC-conjugated gelatin, PMA-treated and then stained with phalloidin. The white dashed line is the outline of the cell boundary and is traced here as a guide to the eye. White arrows indicate the areas in which gelatin was degraded by individual podosomes or podosome rosettes. Scale bars, 10 μm. (**e**,**f**) *Ex vivo* VEGF-A stimulation induces podosome rosettes in aortic vessels. Aortic explants were incubated for 48 h in M199 10% FCS (unstimulated) or M199 10% FCS with 30 ng ml^{-1} of VEGF-A (48 h VEGF-A). (**e**) Immunostaining of a representative 48 h VEGF-A-stimulated aortic explant. Inset, a podosome rosette. Scale bar, 20 μm. Single-channel images are in Supplementary Fig. 1e. (**f**) Graph showing the percentage of podosome-rosette-positive ECs in the endothelial layer of aortic explants. Mean ± s.e.m. of $n=3$ independent experiments in which 511 nuclei were analysed per experimental point. (**b**,**c**,**f**) Statistical significance was calculated using an unpaired non-parametric Mann–Whitney test (** $P<0.01$ versus unstimulated.).

structures: individual podosomes or multiple podosomes clustered into podosome rosettes[7,11,12] (Fig. 1a). Both structures were rarely present in cultured ECs but their amount can be increased with phorbol-12-myristate-13-acetate (PMA) treatment[12,13] (Fig. 1a). We evaluated whether the number of cells carrying individual podosomes or podosome rosettes was altered in angiogenic endothelium by comparing ECs that were previously stimulated or not with VEGF-A for 24 h. The number of podosome-rosette-containing ECs gradually increased over time and was significantly higher in angiogenic than in quiescent ECs (Fig. 1b and Supplementary Fig. 1a,b). Conversely, the number of ECs carrying individual podosomes was not influenced (Fig. 1b). Moreover, we observed self-organizing podosome rosettes in angiogenic LifeAct–RFP-transduced[14] ECs (Supplementary Video 1).

As MT1-MMP is considered the main ECM proteinase in podosomes[7,15,16], we quantified the active form of MT1-MMP by flow cytometry. The amount of active MT1-MMP in angiogenic ECs gradually increased during PMA treatment (Supplementary Fig. 1c) and, after 40 min, it was 1.8-fold higher in angiogenic

© 2014 Macmillan Publishers Limited. All rights reserved.

compared with quiescent ECs (Fig. 1c). Moreover, larger areas of gelatin degradation—previously associated with podosomes[13]—were present in cells with podosome rosettes compared with individual podosomes (Fig. 1d).

To investigate whether endothelial podosome rosettes were present not only in cultured angiogenic ECs but also in vascular angiogenic endothelium, we analysed mouse aortic explants *ex vivo*-treated with VEGF-A for 48 h (Supplementary Fig. 1d). VEGF-A-stimulated aortae exhibited podosome rosettes, identified as circular F-actin- and cortactin-containing structures localized on the basal side of the endothelial layer (Fig. 1e and Supplementary Fig. 1d,e). In agreement with our *in vitro* observation, the number of cells with rosettes significantly increased in the endothelial layer of VEGF-A-stimulated aortae compared with unstimulated samples (Fig. 1f).

Tumour angiogenic vessels are characterized by high levels of functional endothelial podosome rosettes

To investigate the presence of podosome rosettes in adult vessels undergoing *in vivo* angiogenesis, we analysed several tissues: two mouse models of tumour angiogenesis—the xenograft of B16F10 melanoma[17] and the RipTag2 genetic model of pancreatic insulinoma[3]; a mouse model of post-ischaemic angiogenesis—the hindlimb ischaemia on gastrocnemius muscles[18,19]; and human clinical biopsies from lung tumours where high vascularity correlates with tumour progression[20]. In all tissues we were able to detect F-actin- and cortactin-positive ring-like structures in the EC membrane in close contact with vBM (Fig. 2a and Supplementary Fig. 2a–c). Notably, F-actin/cortactin rings were characterized by the absence or reduction of laminin staining in vBM (Fig. 2a and Supplementary Fig. 2d). This suggests that vBM components could be locally degraded. Indeed, *in situ* zymography[21] on RipTag2 tumour slices revealed gelatinase activity in the regions that contained F-actin ring-like structures and were simultaneously devoid of laminin staining (Fig. 2b and Supplementary Fig. 2e,f). Podosome rosettes in tumour and ischaemic vessels had a mean diameter of (2.7 ± 0.7) μm (Fig. 2a and Supplementary Fig. 2c) and revealed the presence of podosomal markers, such as dynamin, phospho-FAK, phospho-cortactin and MT1-MMP (Supplementary Fig. 3a).

RipTag2 mice tumours are characterized by an angiogenic switch phase[3,22]. We visualized and quantified the number of endothelial podosome rosettes in tumour vasculature at different stages of tumour progression (Fig. 2c and Supplementary Fig. 3b). Whereas quiescent capillaries of normal islets were characterized by a negligible level of rosettes, the density of rosettes was strongly and significantly increased during the transition from the hyperplastic to the *in situ* tumour stage (Fig. 2c). Moreover, by measuring podosome rosettes in human lung tumour biopsies, we found that endothelial podosome rosette density is correlated with microvessel density and VEGF-A quantity (Fig. 2d,e and Supplementary Fig. 3c). Therefore, it seems that tumour angiogenic endothelium is characterized by a high number of ECM-degrading podosome rosettes.

$\alpha_6\beta_1$ integrin is essential for VEGF-induced endothelial podosome rosettes

Integrins are known to be involved in podosome formation[7,16,23–25]. Most of the integrins expressed in ECs were recruited in podosome rosettes of angiogenic ECs (Fig. 3a and Supplementary Fig. 4a). To investigate whether these integrins are functionally implicated in rosette formation, we treated angiogenic ECs with specific function blocking antibodies. The inhibition of $\alpha_1\beta_1$, $\alpha_2\beta_1$, $\alpha_4\beta_1$, $\alpha_6\beta_1$ or $\alpha v\beta_3$ significantly impaired podosome rosette formation, suggesting a specific role for these integrins in rosette dynamics. Notably, only the $\alpha_6\beta_1$ inhibition completely blocked the VEGF-induced rosette formation (Fig. 3a,b), impairing, in turn, MT1-MMP membrane localization and gelatin degradation (Fig. 3c and Supplementary Fig. 4b). Interestingly, individual podosomes were not affected by the anti-$\alpha_6\beta_1$ treatment (Supplementary Fig. 4c). We confirmed the $\alpha_6\beta_1$ involvement in rosette formation by silencing the α_6 subunit (Supplementary Fig. 4d). Angiogenic ECs with reduced $\alpha_6\beta_1$ integrin levels failed to form podosome rosettes (Fig. 3d). Furthermore, consistent with previous results[26,27], VEGF stimulation strongly upregulated the expression of α_6 integrin in ECs (Supplementary Fig. 4e), thus pointing to $\alpha_6\beta_1$ as a potential effector acting downstream of VEGF in the signalling pathway that drives rosette formation.

Integrin $\alpha_6\beta_1$ was gradually recruited in podosome rosettes during their formation (Supplementary Fig. 5a); we therefore speculated that $\alpha_6\beta_1$ levels in endothelial podosome rosettes could correlate with their stability. To test this hypothesis, we analysed the lifespan of podosomes composing the rosettes in integrin α_6–GFP (α_6–GFP) and LifeAct–RFP-expressing ECs. Podosomes with high levels of integrin $\alpha_6\beta_1$ exhibited significantly longer lifespans than podosomes with low $\alpha_6\beta_1$ integrin (Fig. 3e and Supplementary Fig. 5b), confirming a crucial role for integrin α_6 in the stability of podosomes in rosettes.

We then analysed α_6 localization in VEGF-A-stimulated aortic explants. Integrin α_6 co-localized with F-actin/cortactin ring-like structures in the basal side of the endothelial layer (Fig. 3f and Supplementary Fig. 5c), and lentiviral-mediated downregulation of α_6 integrin in whole aortic explants significantly impaired rosette formation (Supplementary Fig. 5d). Moreover, experiments with aortic explants from Tie2-dependent integrin α_6 null mice[19] showed that genetic ablation of endothelial α_6 completely suppressed the formation of endothelial rosettes (Fig. 3g).

Laminin impairs endothelial podosome rosette formation

To gain insight into the function of $\alpha_6\beta_1$ integrin in rosette formation, we investigated the role of laminin, the main $\alpha_6\beta_1$ ligand[26]. Unexpectedly, plating ECs on laminin severely inhibited VEGF-A-induced rosette formation and strongly decreased the level of active MT1-MMP (Fig. 4a,b), but did not reduce the number of individual podosomes (Supplementary Fig. 6a). On the basis of these observations, we expected that laminin ablation from vBM could increase the number of podosome rosettes in blood vessels. To directly test this hypothesis, we stimulated with VEGF-A aortic explants isolated from α_4 laminin subunit null mice[28,29] (*Lama4*$^{-/-}$). Laminin α_4 is a component of laminin-411, one of the main laminins in vBM (refs 28,29). Genetic ablation of laminin α_4 significantly increased VEGF-A-induced formation of rosettes in ECs of aortic explants (Fig. 4c).

Interestingly, in ECs plated on laminin, the remaining podosome rosettes contained a significantly reduced amount of $\alpha_6\beta_1$ integrin (Supplementary Fig. 6b). Therefore, we evaluated whether the level

© 2014 Macmillan Publishers Limited. All rights reserved.

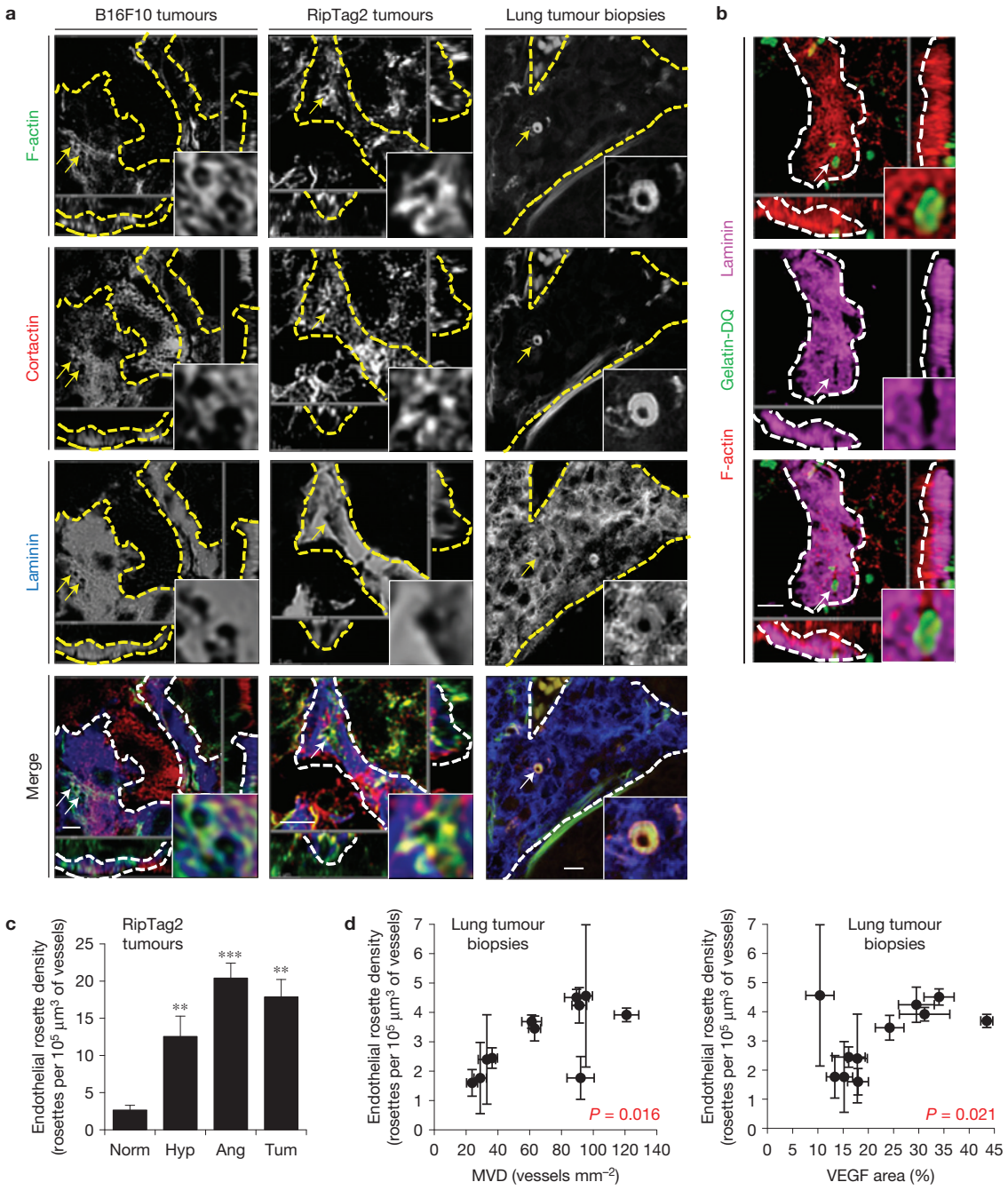

Figure 2 Tumour angiogenic vessels are characterized by high levels of endothelial podosome rosettes. (**a**) Confocal imaging stacks of representative vessels in subcutaneous B16F10 melanoma, in angiogenic islets of transgenic RipTag2 mice or human samples of lung tumours. *xyz*-section of immunostaining for primary antibodies as indicated. Vessels are delimited by dashed lines; arrows indicate podosome rosettes. Inset, the podosome rosette. Schematization and 3D rendering in Supplementary Fig. 2a,b. Scale bars, 10 µm. (**b**) *In situ* zymography in RipTag2 angiogenic islets. *xyz*-section of staining for primary antibodies as indicated and gelatin-DQ (dye-quenched), showing the degradated gelatin. Vessels are delimited by white dashed lines; white arrows indicate podosome rosettes. Inset, the podosome rosette. 3D rendering in Supplementary Fig. 2e. Scale bar, 10 µm. (**c**) Graph shows the density of podosome rosettes in vessels of RipTag2 tumour mouse stages. Vessel regions of interest were determined with laminin staining. Mean ± s.e.m. of $n=3$ mice, 5 fields per tumour stage. Statistical significance was calculated using a one-way ANOVA test followed by Bonferroni-adjusted *post hoc* *t*-tests ($^{**}P<0.01$ versus normal islets; $^{***}P<0.001$ versus normal islets). (**d**) Scatter plots of the density of endothelial podosome rosettes versus microvessel density (MVD)-CD31 ($r^2=0.49$, $P=0.016$) and VEGF area fraction in biopsy samples of lung tumours ($r^2=0.46$, $P=0.021$). Mean ± s.e.m. of $n=3$ different vessels per biopsy for rosette density and $n=20$ fields per slide for MVD and VEGF. Statistical significance was calculated using a Pearson correlation test. Representative images are shown in Supplementary Fig. 3c.

of $\alpha_6\beta_1$ on the cell surface was modulated by laminin. We observed a pronounced reduction of membrane α_6–GFP, but not of total α_6–GFP, on PMA treatment in the absence of laminin (Fig. 4d and Supplementary Fig. 6c,d). In contrast, when ECs were plated on

© 2014 Macmillan Publishers Limited. All rights reserved.

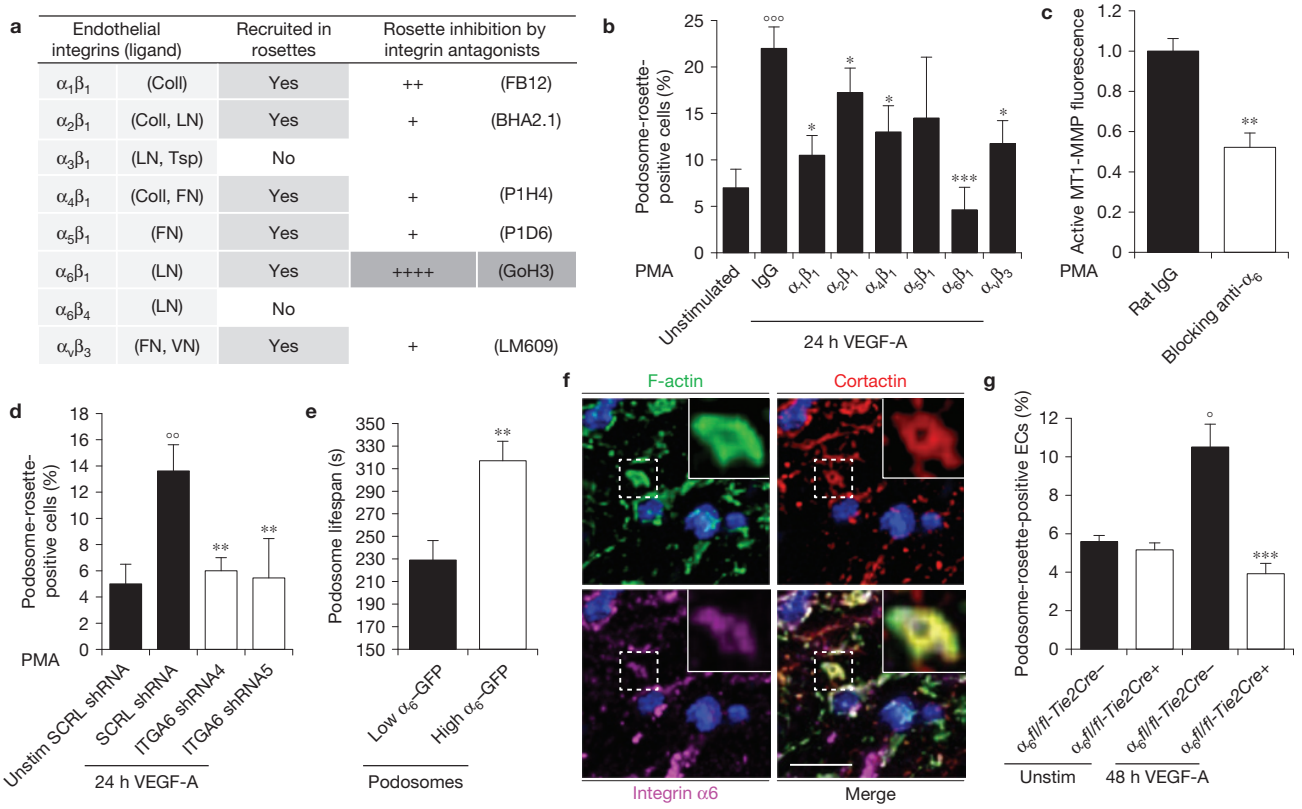

Figure 3 Integrin α_6 is essential for VEGF-induced endothelial podosome rosette formation and function. (**a**) Table of integrin recruitment in endothelial podosome rosettes and functional blocking treatment. The qualitative analysis of rosette blockade is based on podosome-rosette-positive cells percentages in comparison with aspecific IgG treatment. Confocal micrographs of integrin recruitment are shown in Supplementary Fig. 4a. (**b**) Graph showing the percentages of podosome-rosette-positive ECs, stimulated as indicated and treated with aspecific IgG or anti-integrin blocking antibodies 2 h before PMA treatment. ECs were treated with IgG or anti-integrin blocking antibody (20 μg ml^{-1}) during cell adhesion and then stimulated with PMA for 30 min. Mean ± s.e.m. of $n=3$ independent experiments in which 250 cells were analysed per experimental point. Statistical significance was calculated using a one-way ANOVA test followed by Bonferroni-adjusted *post hoc t*-tests ($^{\circ\circ\circ}P<0.001$ versus unstimulated; $^{*}P<0.05$ versus 24 h VEGF-A IgG; $^{***}P<0.001$ versus 24 h VEGF-A IgG). (**c**) Cytofluorimetric analysis of active MT1-MMP in VEGF-A-stimulated ECs, treated with rat IgG or anti-α_6 blocking antibody and then stimulated with PMA for 30 min. Normalized mean ± s.e.m. of $n=3$ independent experiments in which 9×10^4 cells were analysed per experimental point. Statistical significance was calculated using an unpaired non-parametric Mann–Whitney test ($^{**}P<0.01$ versus rat IgG). (**d**) Graph showing the percentages of podosome-rosette-positive ECs, transduced with scramble (SCRL) shRNA or shRNA against integrin α_6 (ITGA6 shRNA4 and ITGA6 shRNA5). Membrane integrin α_6 levels in transduced ECs are shown in Supplementary Fig. 4d. Mean ± s.e.m. of $n=3$ independent experiments in which 250 cells were analysed per experimental point. Statistical significance was calculated using a one-way ANOVA test followed by Bonferroni-adjusted *post hoc t*-tests ($^{\circ\circ}P<0.01$ versus Unstim SCRL shRNA; $^{**}P<0.01$ versus SCRL shRNA). (**e**) Lifespan of the podosomes that form endothelial rosettes in α_6–GFP- and LifeAct–RFP-transduced ECs. Graph shows the lifespan in minutes of podosomes with low or high levels of integrin α_6 detected with TIRF microscopy (90 nm of depth) in VEGF-stimulated ECs. Mean ± s.e.m. of $n=230$ podosomes from 3 different cells. Statistical significance was calculated using an unpaired non-parametric Mann–Whitney test ($^{**}P<0.01$ versus low ITGA6). (**f**) Endothelial layer of a 48 h VEGF-A-stimulated aortic explant immunostained by the indicated antibodies and nuclear-stained by DAPI (blue). Inset, a podosome rosette in the basal side of the endothelial layer. Scale bar, 20 μm. (**g**) VEGF-A stimulation in aortic explants of Tie2-dependent α_6 null mice. Aortic explants from WT (α_6*fl/fl-Tie2Cre*–) or endothelial α_6 null (α_6*fl/fl-Tie2Cre*+) mice were incubated for 48 h in M199 10% FCS (unstim) or M199 10% FCS with 30 ng ml^{-1} of VEGF-A (48 h VEGF-A). Mean ± s.e.m. of $n=3$ independent experiments in which 1,250 nuclei were analysed per experimental point. Statistical significance was calculated using two-way ANOVA test followed by Bonferroni-adjusted *post hoc t*-tests ($^{\circ}P<0.05$ versus unstim α_6*fl/fl-Tie2Cre*–; $^{***}P<0.001$ versus 48 h VEGF-A α_6*fl/fl-Tie2Cre*–).

laminin, the levels of α_6–GFP at the cell surface were not modulated by PMA stimulation (Fig. 4d). Taken together, these results suggest that, when bound to $\alpha_6\beta_1$, laminin blocks this integrin in plasma membrane and, in turn, inhibits rosette formation.

Laminin slows down $\alpha_6\beta_1$ integrin translocation from FAs to podosome rosettes

To further define the relationship between $\alpha_6\beta_1$ integrin dynamics and podosome rosettes, we imaged α_6–GFP and LifeAct–RFP-transduced ECs. During PMA treatment, ECs seeded on laminin formed only classical $\alpha_6\beta_1$-containing FAs (FAs), but not podosome rosettes. In the absence of laminin, $\alpha_6\beta_1$ was instead massively recruited into podosome rosettes that underwent dynamic cycles of continuous assembly and disassembly (Supplementary Video 2). Laminin thus favours the localization of $\alpha_6\beta_1$ into FAs rather than into podosome rosettes (Supplementary Fig. 6e).

To better characterize the reorganization of adhesion sites during rosette formation, we analysed vinculin–RFP-transfected ECs by total internal reflection fluorescence (TIRF) microscopy. Before PMA treatment, vinculin was localized into FAs (Fig. 5a and

© 2014 Macmillan Publishers Limited. All rights reserved.

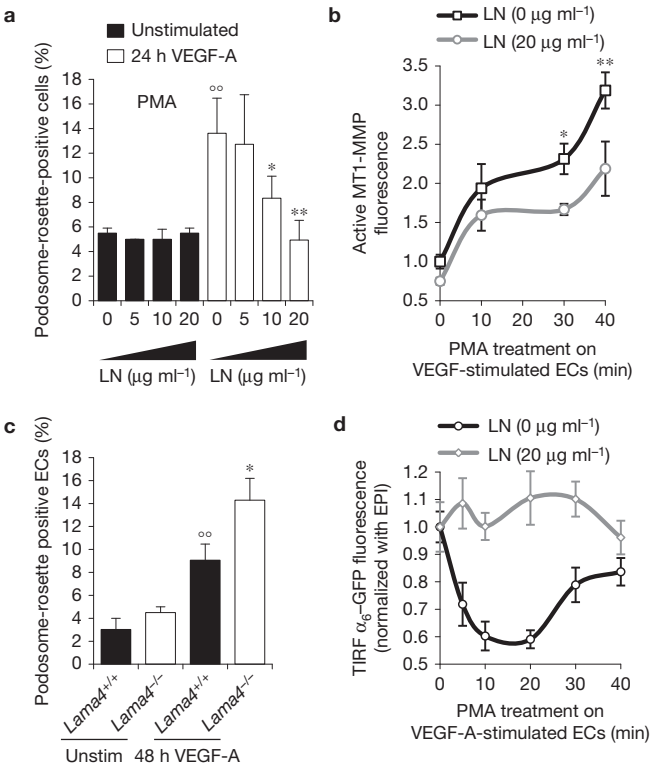

Figure 4 Laminin impairs podosome rosette formation. (**a**) Graph showing the percentages of podosome-rosette-positive ECs, stimulated as indicated, seeded on gelatin-coated coverslips with the indicated addition of laminin. Percentages of individual-podosome-positive cells are in Supplementary Fig. 6a. Mean ± s.e.m. of $n=3$ independent experiments in which 260 cells were analysed per experimental point. Statistical significance was calculated using a two-way ANOVA test followed by Bonferroni-adjusted *post hoc t*-tests ($^{\circ\circ}P<0.01$ versus unstimulated; $^{*}P<0.05$ versus LN (0 μg ml^{-1}); $^{**}P<0.01$ versus LN (0 μg ml^{-1})). (**b**) Cytofluorimetric analysis of active MT1-MMP in VEGF-stimulated ECs, seeded on a gelatin coating with the indicated addition of laminin. Normalized mean ± s.e.m. of $n=3$ independent experiments in which 10^5 cells were analysed per experimental point. Statistical significance was calculated using a two-way ANOVA test followed by Bonferroni-adjusted *post hoc t*-tests ($^{*}P<0.05$ versus LN (0 μg ml^{-1}); $^{**}P<0.01$ versus LN (0 g ml^{-1})). (**c**) VEGF-A stimulation in aortic explants of laminin α_4 null mice. Aortic explants from *Lama4*$^{+/+}$ or *Lama4*$^{-/-}$ mice were incubated for 48 h in M199 10% FCS (unstim) or M199 10% FCS with 30 ng ml^{-1} of VEGF-A (48 h VEGF-A). Mean ± s.e.m. of $n=3$ independent experiments in which 550 nuclei were analysed per experimental point. Statistical significance was calculated using a two-way ANOVA test followed by Bonferroni-adjusted *post hoc t*-tests ($^{\circ\circ}P<0.05$ versus unstimulated *Lama4*$^{+/+}$; $^{*}P<0.05$ versus 48 h VEGF-A *Lama4*$^{+/+}$). (**d**) Integrin α_6 membrane localization is modulated by laminin in the substratum. The graph shows the ratio of α_6–GFP fluorescence in the membrane (TIRF microscopy with <90 nm of deepness) and in the whole cell (epifluorescence, EPI) in the indicated periods of PMA treatment; mean ± s.e.m. of $n=30$ cells from 3 independent experiments.

Supplementary Video 3). After PMA treatment, roughly all FAs disassembled and only a few focal complexes were still visible; then the formation of podosome rosettes became detectable (Fig. 5a and Supplementary Video 3). These results suggest that FA and podosome rosette dynamics are indeed correlated phenomena. Therefore, we studied rosettes in ECs treated with drugs able to modulate FA dynamics. First, we examined whether—as previously suggested[7,9]—the formation of podosome rosettes is independent of direct *de novo* protein synthesis, and we found that the protein-translation inhibitor cycloheximide did not interfere with the induction of rosettes (Fig. 5b). In contrast, the microtubule inhibitor nocodazole completely blocked the appearance of podosome rosettes. As nocodazole stabilizes FA and its ensuing removal results instead in FA disassembly[30], we observed that nocodazole washout, besides favouring FA dismantling, significantly increased the formation of podosome rosettes on PMA treatment. Furthermore, challenging ECs with the recycling inhibitor primaquine extensively impaired the development of podosome rosettes (Fig. 5b) and completely blocked the stimulatory effect of nocodazole washout on rosette formation (Fig. 5b). These results support a model where FA components need to be trafficked to nascent podosome rosettes to allow the formation of the latter (Supplementary Fig. 6f).

The requirement for a PMA-elicited reorganization of ECM adhesions could explain why the binding of laminin to $\alpha_6\beta_1$ integrin, which stabilizes this integrin in FAs, inhibits podosome rosettes. To confirm this hypothesis, we forced FA disassembly in ECs seeded on laminin. Microtubule-induced FA disassembly was sufficient to rescue the inhibitory effect of laminin on rosette formation (Fig. 5c), not affecting individual podosomes (Supplementary Fig. 6g). Taken together, these results suggest that the level of available $\alpha_6\beta_1$ integrin is a limiting factor for endothelial podosome rosette formation. We therefore analysed rosette incidence in ECs with different levels of $\alpha_6\beta1$ integrin and seeded on different amounts of laminin. α_6-silenced ECs failed to form rosettes independently of laminin concentration, whereas $\alpha_6\beta_1$-overexpressing ECs showed a high number of rosettes even when seeded on elevated concentrations of laminin (Fig. 5d). Conversely, modulation of $\alpha_6\beta_1$ integrin levels did not affect individual podosomes (Supplementary Fig. 6h). Moreover, the overexpression of α_6 alone was sufficient to promote rosette formation in the absence of VEGF even in cells adhering on laminin (Fig. 5e).

Endothelial podosome rosettes are precursors of new vessel branching points

The presence of endothelial rosettes in the angiogenic endothelium prompted us to investigate their role in sprouting angiogenesis and vessel branching. We studied the formation of podosome rosettes in the mouse aortic ring (mAR) assay[26,31]. This *ex vivo* angiogenesis model is characterized by the formation of VEGF-dependent capillary-like structures producing a vBM sleeve[32] (Supplementary Fig. 7a). Ring-like structures with F-actin/cortactin/MT1-MMP co-localization were detectable in angiogenic sprouts. These ECM-degradative 4-μm-diameter structures were localized in the basal side of ECs (Fig. 6a,b and Supplementary Fig. 7b,c) and are also characterized by localization of integrin α_6 (Supplementary Fig. 7d). Interestingly, the levels of α_6 integrin on the surface of cells containing rosettes, but outside the rosette, were reduced compared with cells without rosettes (Supplementary Fig. 7e,f). This supports the hypothesis of a re-localization of α_6 from the cell surface to endothelial rosettes.

Notably, the localization of podosome rosettes in mAR sprouts was distal from the tip cell (Fig. 6b and Supplementary Video 4), suggesting that these structures were not necessarily involved in tip cell migration, but possibly in the process of branching from pre-existing sprouts. To validate this hypothesis, we performed live-imaging studies on podosome rosettes and lateral vessel branching

© 2014 Macmillan Publishers Limited. All rights reserved.

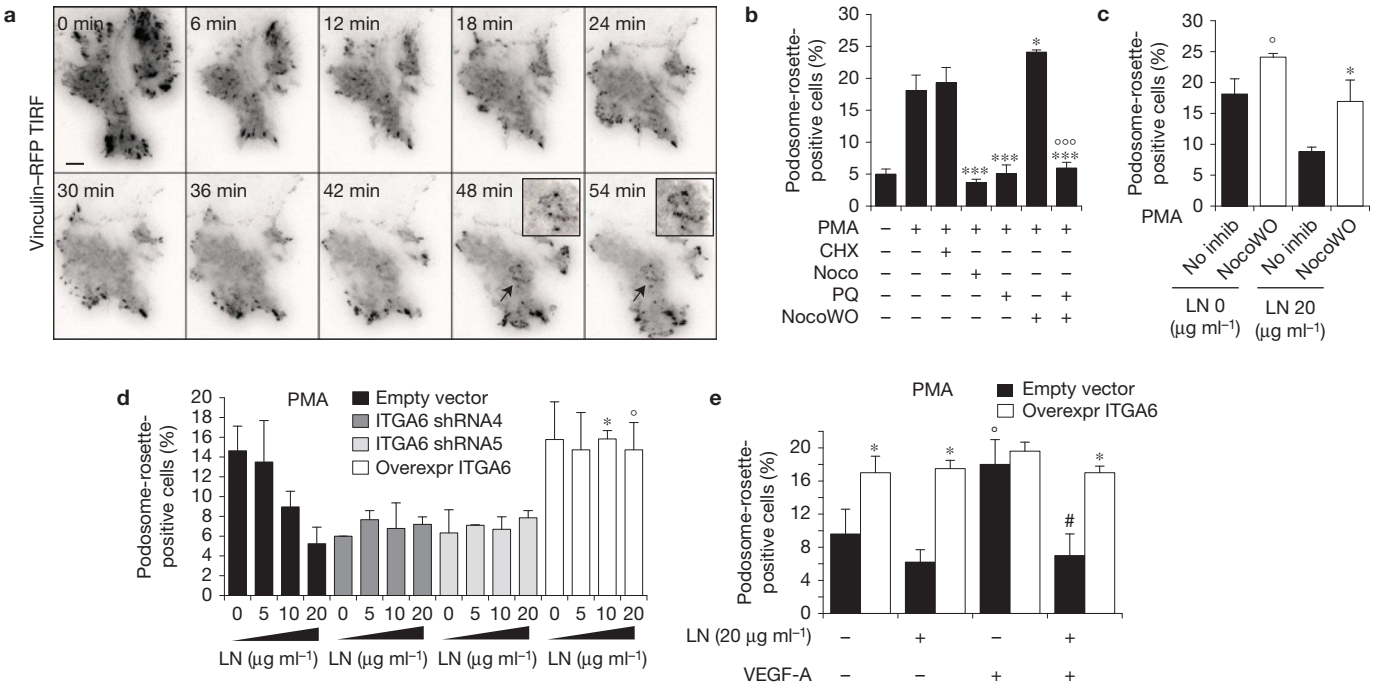

Figure 5 α_6 integrin–laminin binding in FAs slows down α_6 integrin translocation to podosome rosettes. (**a**) Time-lapse TIRF microscopy of vinculin–RFP-transfected ECs during PMA treatment. Insets, podosome rosettes indicated by arrows. For complete video, see Supplementary Video 3. Scale bar, 20 μm. (**b**) Graph showing the percentages of podosome-rosette-positive ECs, treated as indicated. CHX: cycloheximide; Noco: nocodazole; PQ: primaquine; NocoWO: nocodazole washout. Mean ± s.e.m. of $n=3$ independent experiments in which 200 cells were analysed per experimental point. Statistical significance was calculated using a one-way ANOVA test followed by Bonferroni-adjusted *post hoc* *t*-tests $^{***}P<0.05$ versus PMA treated; $^{***}P<0.001$ versus PMA treated; $^{\circ\circ\circ}P<0.001$ versus NocoWO+PMA). (**c**) Graph showing the percentages of podosome-rosette-positive ECs, seeded on gelatin-coated coverslips with the indicated laminin addition and PMA-stimulated with or without nocodazole washout. Percentages of individual-podosome-positive cells are in Supplementary Fig. 6g. Mean ± s.e.m. of $n=3$ independent experiments in which 230 cells were analysed per experimental point. Statistical significance was calculated using a two-way ANOVA test followed by Bonferroni-adjusted *post hoc* *t*-tests ($^{\circ}P<0.05$ versus no inhib LN (0 μg ml^{-1}); $^{*}P<0.05$ versus no inhib LN (20 μg ml^{-1})). (**d**) Graph showing the percentages of podosome-rosette-positive ECs, seeded on gelatin-coated coverslips with the indicated addition of laminin. ECs were transduced as indicated. Membrane integrin α_6 levels in transduced ECs are shown in Supplementary Fig. 4d. Percentages of individual-podosome-positive cells are in Supplementary Fig. 6h. Mean ± s.e.m. of $n=3$ independent experiments in which 320 cells were analysed per experimental point. Statistical significance was calculated using one-way ANOVA test followed by Bonferroni-adjusted *post hoc* *t*-tests ($^{*}P<0.05$ versus empty vector L(10 μg ml^{-1}); $^{\circ}P<0.05$ versus empty vector L(20 μg ml^{-1}). (**e**) Graph showing the percentages of podosome-rosette-positive ECs, seeded on gelatin-coated coverslips with 20 μg ml^{-1} laminin. ECs were transduced as indicated and stimulated or not with VEGF-A for 24 h. Mean ± s.e.m. of $n=3$ independent experiments in which 420 cells were analysed per experimental point. Statistical significance was calculated using a two-way ANOVA test followed by Bonferroni-adjusted *post hoc* *t*-tests ($^{*}P<0.05$ versus its corresponding empty vector; $^{\circ}P<0.05$ versus empty vector L-VEGF-A−; # $P<0.05$ versus empty vector L-VEGF-A+).

by exploiting LifeAct–EGFP-expressing transgenic mice[33]. All lateral branches analysed in our study were preceded by the formation of *bona fide* podosome rosettes (Fig. 6c,d and Supplementary Fig. 7f and Supplementary Videos 5 and 6). However, a modest percentage of rosettes (0.5%) effectively produced new sprouts, suggesting that the appearance of rosettes alone is not sufficient to induce lateral branching.

We then analysed mAR branching in the absence of integrin α_6 or laminin. Genetic ablation of endothelial α_6 significantly reduced both the rosette formation (Fig. 3g) and the branching incidence of angiogenic sprouts (Fig. 6e and Supplementary Video 7) without changing the total sprouting length (Supplementary Fig. 7g). Conversely, branching of *Lama4*$^{-/-}$ mARs was significantly enhanced (Fig. 6f and Supplementary Video 8), but the sprout length was not modified (Supplementary Fig. 7h). Moreover, the exogenous addition of laminin rescued the hyper-branched phenotype of *Lama4*$^{-/-}$ mARs (Fig. 6f and Supplementary Video 9).

In vivo blocking of $\alpha_6\beta_1$ integrin impairs endothelial podosome rosette formation and reduces tumour vessel branching

To understand the physio-pathological relevance of endothelial podosome rosettes in the angiogenic process, we treated RipTag2 mice with the anti-α_6 blocking antibody. We first tested the accessibility of anti-α_6 to endothelial podosome rosettes[26,34]. Ten minutes after injection in RipTag2 mice, the anti-α_6 antibody was sharply localized in podosome rosettes of tumour blood vessels (Fig. 7a and Supplementary Fig. 7i).

To evaluate the effects of anti-α_6 on endothelial rosettes, we treated RipTag2 mice for 2 weeks by starting antibody administration at the beginning of the angiogenic stage. The blockade of $\alpha_6\beta_1$ integrin caused a strong reduction of podosome rosette density (Fig. 7a) and concomitantly a decrease of vessel branching (Fig. 7c).

To confirm the results obtained with anti-α_6 treatment, we analysed rosette density in vessels of B16F10 xenograft and ischaemic tissues from endothelial α_6 integrin null mice. Genetic endothelial

© 2014 Macmillan Publishers Limited. All rights reserved.

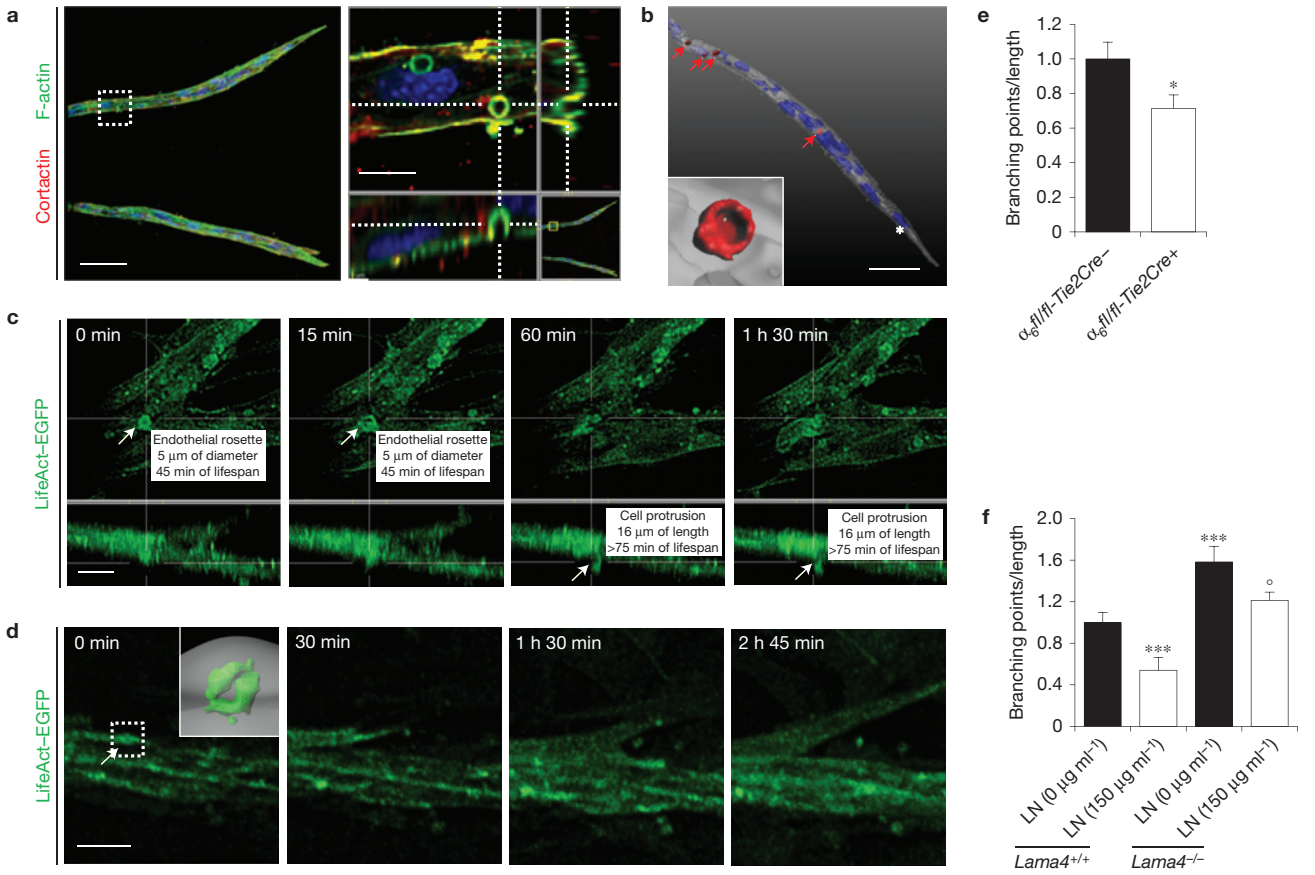

Figure 6 Endothelial podosome rosettes precede vessel branching from a pre-existing vessel. (**a**) Confocal image stacks of representative angiogenic outgrowths from 7-day mARs into collagen gel (left panel). Scale bar, 50 μm. Right panel, *xyz*-section of the white dotted square in the left panel. Scale bar, 10 μm. (**b**) 3D isosurface rendering of endothelial rosettes in angiogenic outgrowths. Angiogenic outgrowths (grey) and podosome-rosettes (red) were recognized with co-localization of F-actin/cortactin staining (indicated by red arrows) as detailed in the Supplementary Methods. The white asterisk indicates the tip-cell nucleus. Inset, a representative endothelial rosette. For complete video, see Supplementary Video 4. Scale bar, 30 μm. (**c**,**d**) Time-lapse multiphoton microscopy of angiogenic outgrowths from LifeAct–EGFP mARs. For complete video, see Supplementary Videos 5 and 6. The podosome rosette and cell protrusion are indicated by white arrows. Scale bar, 20 μm in **c** and 50 μm in **d**. (**e**) Branching density—number of branching points divided by vascular area—of angiogenic outgrowths from WT (α_6*fl/fl-Tie2Cre*–) or endothelial α_6 null (α_6*fl/fl-Tie2Cre*+) mARs. Dynamical analysis of branching shown in Supplementary Video 7. Mean ± s.e.m. of $n=18$ mARs, 3 mARs per mouse from 6 mice. Statistical significance was calculated using a two-way ANOVA test followed by Bonferroni-adjusted *post hoc t*-tests ($^{*}P<0.05$ versus α_6*fl/fl-Tie2Cre*–). (**f**) Branching density of angiogenic outgrowths from laminin α_4 null mARs into collagen with or without laminin addition. Dynamical analysis of *Lama4*$^{-/-}$ branching is shown in Supplementary Video 8 and laminin in gel in Supplementary Video 9. Mean ± s.e.m. of $n=8$ mARs, 2 mARs per mouse from 4 mice. Statistical significance was calculated using a two-way ANOVA test followed by Bonferroni-adjusted *post hoc t*-tests ($^{***}P<0.001$ versus LN (0 μg ml^{-1}) WT; $^{\circ}P<0.05$ versus LN (0 μg ml^{-1}) *Lama4*$^{-/-}$).

ablation of α_6 integrin effectively impaired podosome rosettes in both models (Fig. 7d,e). B16F10 tumours showed that α_6 integrin ablation significantly reduced blood vessel branching in tumours (Fig. 7f), confirming our *ex vivo* results (Fig. 6e). Notably, integrin α_6 localized to podosome rosettes also in angiogenic vessels of human lung tumours (Supplementary Fig. 7l).

DISCUSSION

In the adult organism, blood vessels are usually quiescent and rarely form new branches. ECs and mural cells share a vBM that forms a sleeve around endothelial tubules and prevents resident ECs from leaving their positions[4,35,36]. However, ECs are able to promptly respond to angiogenic signals. The mechanisms controlling vBM proteolytic breakdown and selection of the ECs that steer lateral branches are still poorly understood. Here, we show that angiogenic endothelium forms subcellular structures with degradative activity, called podosome rosettes, which precede the emergence of new lateral sprouts.

It is known that MMPs—including MT1-MMP—correlate with angiogenesis, by letting ECs breach the vBM and enter tissues[6,37]. Spatial and temporal control of these proteinases is essential for an efficient sprouting. In angiogenic ECs podosome rosettes are plasma membrane regions where MT1-MMP is enriched. Indeed, it is reasonable that constrained degradation of vBM is preferable to diffuse and uncontrolled proteinase activity.

Furthermore, podosome rosettes are also adhesive structures containing integrins. Notably, in a model of BM invasion in *Caenorhabditis elegans*[38], the integrin heterodimer INA-1/PAT-3—highly homologous with mammalian $\alpha_6\beta_1$—is crucial for cell invasion through BM (ref. 38). Here we show that the assembly of podosome

© 2014 Macmillan Publishers Limited. All rights reserved.

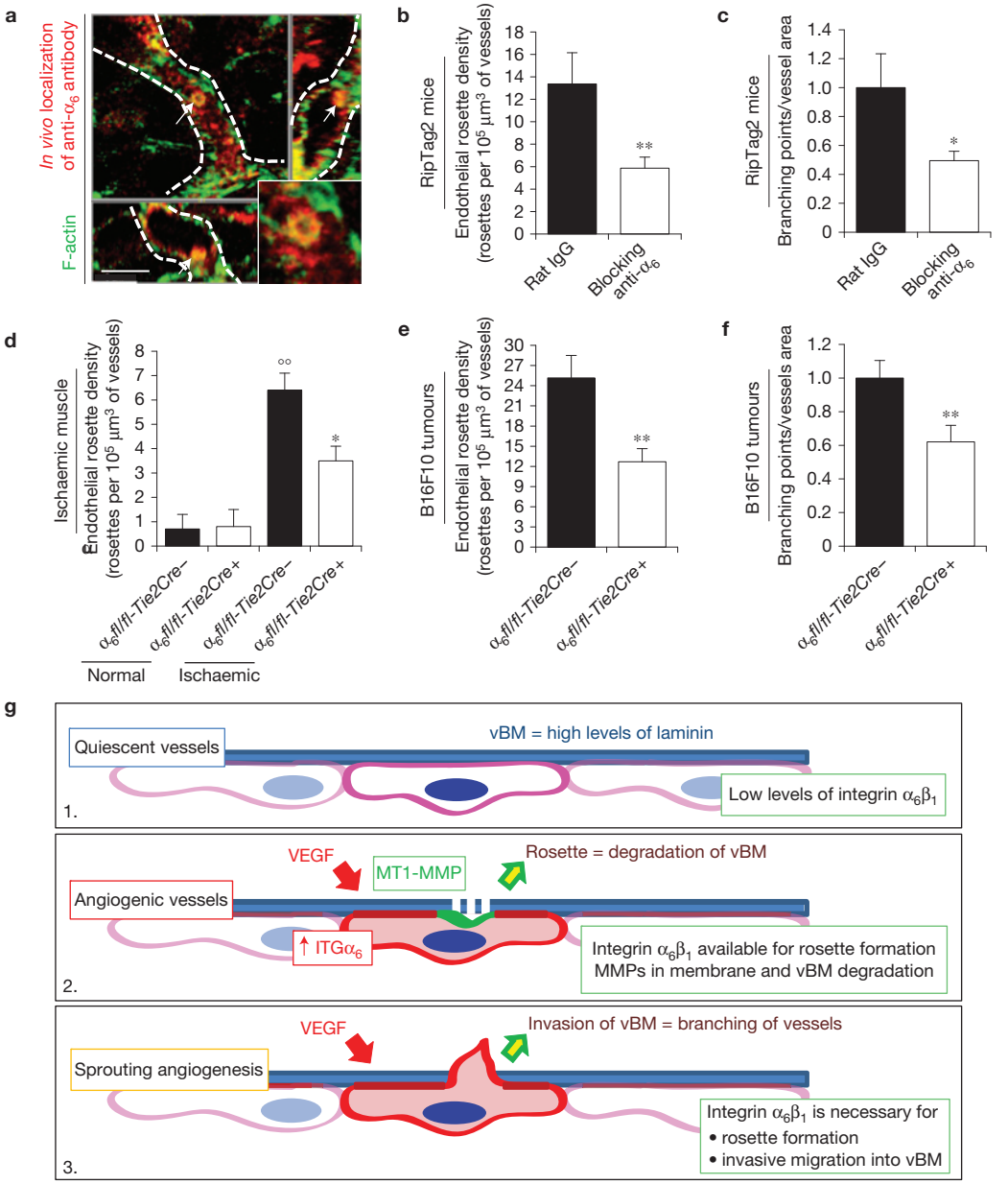

Figure 7 *In vivo* blocking of integrin α_6 impairs endothelial podosome rosette formation and reduces vessel branching in tumours. (**a**) Rapid accumulation of anti-α_6 integrin antibody into endothelial podosome rosettes of RipTag2 tumour vessels. *xyz*-sections of confocal micrographs of the distribution of immunoreactivity in RipTag2 tumours 10 min after intravenous injection of 25 μg of anti-α_6 integrin antibody. Vessels are delimited by white dotted lines; white arrows indicate the podosome rosette. Inset, high magnification of the podosome rosette. Scale bar, 5 μm. (**b**) Measurements of rosette density in vessels of RipTag2 mouse tumours, treated with rat IgG or anti-α_6 blocking antibody. Mean ± s.e.m. of $n = 30$ fields, 5 fields per pancreatic islet from 6 mice per treatment group. Statistical significance was calculated using an unpaired non-parametric Mann–Whitney test ($^{**}P < 0.01$ versus rat IgG.). (**c**) Branching density in blocking anti-α_6-treated RipTag2 tumours. Mean ± s.e.m. of $n = 30$ fields, 5 fields per mouse from 6 mice per treatment group. Statistical significance was calculated using an unpaired non-parametric Mann–Whitney test ($^{*}P < 0.05$ versus rat IgG). (**d**) Measurements of rosette density in vessels of gastrocnemius muscles from unilateral hindlimb ischaemia experiments in WT (α_6*fl/fl-Tie2Cre*−) or endothelial α_6 null (α_6*fl/fl-Tie2Cre*+) mice. Mean ± s.e.m. of $n = 9$ fields, 3 fields per muscle from 3 mice. Statistical significance was calculated using an unpaired non-parametric Mann–Whitney test ($^{\circ\circ}P < 0.01$ versus normal α_6*fl/fl-Tie2Cre*−; $^{*}P < 0.05$ versus α_6*fl/fl-Tie2Cre*+). (**e**) Measurements of rosette density in vessels of subcutaneous B16-F10 tumours in WT (α_6*fl/fl-Tie2Cre*−) or endothelial α_6 null (α_6*fl/fl-Tie2Cre*+) mice. Mean ± s.e.m. of $n = 21$ fields, 3 fields per tumour from 7 mice per treatment group. Statistical significance was calculated using an unpaired non-parametric Mann–Whitney test ($^{**}P < 0.01$ versus α_6*fl/fl-Tie2Cre*−). (**f**) Branching density in B16F10 melanoma subcutaneously injected in Tie2-dependent α_6 KO mice. Mean ± s.e.m. of $n = 42$ fields, 5 fields per tumour from 7 mice per treatment group. Statistical significance was calculated using an unpaired non-parametric Mann–Whitney test ($^{**}P < 0.01$ versus α_6*fl/fl-Tie2Cre*− mice). (**g**) Cartoon showing α_6 integrin/laminin molecular mechanisms involved in sprouting angiogenesis. (1) Quiescent EC have low levels of $\alpha_6\beta_1$ integrin, which binds vBM laminin, is recruited in FAs, and results in blood vessel stabilization. (2) When the tumour produces VEGF, the VEGF induces upregulation of the α_6 integrin subunit in ECs. The increased availability of $\alpha_6\beta_1$ integrin then allows the formation and stabilization of endothelial podosome rosettes and the ensuing MMP-driven degradation of ECM that, in turn, (3) allows vBM invasion by ECs and sprouting angiogenesis.

© 2014 Macmillan Publishers Limited. All rights reserved.

rosettes in ECs depends on $\alpha_6\beta_1$ as well, thus supporting the idea that endothelial podosome rosettes are specialized structures for vBM invasion in vertebrates.

Whereas endothelial podosome rosettes are involved in the sprouting process of vessels embedded in a thick vBM, such as adult vessels, they do not play a relevant role when vBM is absent, such as during early vascular development[39,40]. This might explain why loss of integrin α_6, laminin α_4 or MT1-MMP does not impair vascular development in embryos, but affects pathological angiogenesis in mature tissues[6,19,29].

Importantly, we demonstrated that VEGF-A stimulation induces the assembly of endothelial rosettes, but does not reduce the individual podosomes. This effect largely depends on $\alpha_6\beta_1$ integrin, which is transcriptionally induced by VEGF-A. Recent evidence shows that both FAK and β_1 integrin are required for podosome rosette assembly and stabilization[13,24]. However, the molecular mechanisms leading to the formation of podosome rosettes remain elusive. Here, we show that $\alpha_6\beta_1$ contributes to the stability of podosome rosettes and that high levels of $\alpha_6\beta_1$ are needed within podosome rosettes to increase their lifespans (Fig. 3e).

The transition from a quiescent to a migratory cellular phenotype is often characterized by FA disassembly followed by the formation of invadopodia or podosomes[16,23,41]. Our data, showing that both disassembly of FAs and recycling of their components are necessary for rosette formation, unveil a direct link between FAs and rosettes (Supplementary Fig. 6f). In this context, laminin of vBM hampers rosette formation by sequestering $\alpha_6\beta_1$ in FAs. The upregulation of α_6—induced by angiogenic growth factor stimulation—could overcome the anti-angiogenic effect of vBM by increasing the $\alpha_6\beta_1$ available for the formation of podosome rosettes, which in turn will allow vBM cleavage and angiogenesis.

The molecular actors that modulate adult vasculature geometry are poorly defined. The tortuosity and high branching index of tumour vasculature often make it 'non-functional', characterized by an impaired blood supply[42] and interstitial hypertension[43], which compromise drug delivery[44]. Notably, all angiogenic vessels that we analysed exhibited podosome rosettes but we could not detect them in quiescent vessels. This specific distribution suggests that endothelial podosome rosettes are determinants of angiogenic vessels. Indeed, we showed that inhibition of podosome rosette formation by $\alpha_6\beta_1$ blockade or genetic deletion affects vessel branching (Fig. 6e and Fig. 7c,f). Consistently, previous evidence showed how inhibition or genetic ablation of $\alpha_6\beta_1$ integrin in ECs impaired tumoral and post-ischaemic angiogenesis[19,26]. In contrast, genetic ablation of laminin α_4—described to give hyper-branched angiogenesis in the adult animal—promotes rosette formation and enhances endothelial sprouting[29,45]. The control exerted by $\alpha_6\beta_1$ integrin on tumour blood vessel branching as a consequence of podosome rosette inhibition in ECs supports the previously proposed notion of vascular normalization by suggesting endothelial podosome rosettes as a new target to normalize tumour vasculature.

In summary, this work describes the role of endothelial podosome rosettes as precursors of sprouting angiogenesis and important determinants of the vascular branching in tumour angiogenesis. We proposed a model (Fig. 7g) where quiescent vessels are characterized by low levels of $\alpha_6\beta_1$ integrin, recruited in FAs and bound to the vBM laminin. This hampers the formation of podosome rosettes, reducing the sprouting ability. When a tumour persistently produces VEGF, α_6 integrin is upregulated in ECs. The increased availability of $\alpha_6\beta_1$ integrin allows the formation and stabilization of endothelial podosome rosettes and the ensuing MMP-driven modulation of ECM that, in turn, leads vBM invasion by ECs and sprouting angiogenesis. □

METHODS

Methods and any associated references are available in the online version of the paper.

Note: Supplementary Information is available in the online version of the paper

ACKNOWLEDGEMENTS

A special thank you to E. Georges-Labouesse (CNRS/INSERM/ULP, Illkirch, France), who recently passed away, for kindly providing Tie2-dependent integrin α_6 KO mice. We thank P. C. Marchisio (San Raffaele Scientific Institute, Milano, Italy) for discussion and insightful suggestions on the manuscript; D. R. Sherwood (Duke University Medical Center, Durham, USA) for critical reading of the manuscript; K. Tryggvason (Karolinska Institutet, Stockholm, Sweden) for providing laminin α_4 null mice; R. Wedlich-Söldner (Max-Planck Institute of Biochemistry, Martinsried, Germany) and L. M. Machesky (Beatson Institute for Cancer Research, Glasgow, UK) for providing breeding pairs for the LifeAct–EGFP mouse colony and reagents; R. Falcioni (National Cancer Institute 'Regina Elena', Rome, Italy) for critical reading and reagents; E. De Luca and M. Gai (MBC, Torino, Italy) for their assistance in multiphoton microscopy; Y. Boucher and C. Smith (HMS, Boston, USA) for assistance in immunohistochemistry on human tissues; and E. Giraudo and F. Maione (IRCC, Candiolo, Italy) for their help in the treatment of RipTag2 mice. This work was supported by Associazione Italiana per la Ricerca sul Cancro (AIRC) investigator grants IG (10133, F.B.; 14635, L.P.; 13016 G. Serini) and fellowships (13604 G. Seano; 15026 P.A.G.); AIRC 5x1000 (12182); Converging Technologies Program, grant: 'Photonic Biosensors for Early Cancer Diagnostics'; Technological Platforms for Biotechnology: grant DRUIDI; Fondazione Cassa di Risparmio Torino (CRT); Fondazione Piemontese per la Ricerca sul Cancro-ONLUS (Intramural Grant 5x1000 2008) (L.P.); Fondo Investimenti per la Ricerca di Base RBAP11BYNP (Newton) (F.B. and L.P.); University of Torino-Compagnia di San Paolo: RETHE grant (F.B.); GeneRNet grant (L.P.); P01 CA080124/CA/NCI NIH HHS/United States (R.K.J.); The 'Fondazione T. & L. de Beaumont Bonelli' and the Girardi Family (G. Seano).

AUTHOR CONTRIBUTIONS

G. Seano and L.P. conceived the idea and wrote the manuscript; G. Seano, G.C., P.A.G., A.P. and L.d.B. performed the experiments and analysed the data; L.S. provided LAMA4 mARs; C.B. and D.H. provided endothelial α_6 null mARs, B16F10 tumours and ischaemic tissues; R.K.J. provided human samples; G. Serini, G.T., R.K.J. and F.B. analysed and discussed the data; all authors reviewed and approved the manuscript.

COMPETING FINANCIAL INTERESTS

The authors declare no competing financial interests.

Published online at www.nature.com/doifinder/10.1038/ncb3036
Reprints and permissions information is available online at www.nature.com/reprints

1. Hallmann, R. *et al.* Expression and function of laminins in the embryonic and mature vasculature. *Physiol. Rev.* **85,** 979–1000 (2005).
2. Ferrara, N., Gerber, H. P. & LeCouter, J. The biology of VEGF and its receptors. *Nat. Med.* **9,** 669–676 (2003).
3. Inoue, M., Hager, J. H., Ferrara, N., Gerber, H. P. & Hanahan, D. VEGF-A has a critical, nonredundant role in angiogenic switching and pancreatic beta cell carcinogenesis. *Cancer Cell* **1,** 193–202 (2002).
4. Carmeliet, P. & Jain, R. K. Molecular mechanisms and clinical applications of angiogenesis. *Nature* **473,** 298–307 (2011).
5. Galvez, B. G., Matias-Roman, S., Albar, J. P., Sanchez-Madrid, F. & Arroyo, A. G. Membrane type 1-matrix metalloproteinase is activated during migration of human endothelial cells and modulates endothelial motility and matrix remodeling. *J. Biol. Chem.* **276,** 37491–37500 (2001).
6. Yana, I. *et al.* Crosstalk between neovessels and mural cells directs the site-specific expression of MT1-MMP to endothelial tip cells. *J. Cell Sci.* **120,** 1607–1614 (2007).
7. Linder, S. & Aepfelbacher, M. Podosomes: adhesion hot-spots of invasive cells. *Trends Cell Biol.* **13,** 376–385 (2003).

© 2014 Macmillan Publishers Limited. All rights reserved.

8. Gimona, M., Buccione, R., Courtneidge, S. A. & Linder, S. Assembly and biological role of podosomes and invadopodia. *Curr. Opin. Cell Biol.* **20,** 235–241 (2008).
9. Tarone, G., Cirillo, D., Giancotti, F. G., Comoglio, P. M. & Marchisio, P. C. Rous sarcoma virus-transformed fibroblasts adhere primarily at discrete protrusions of the ventral membrane called podosomes. *Exp. Cell Res.* **159,** 141–157 (1985).
10. Mizutani, K., Miki, H., He, H., Maruta, H. & Takenawa, T. Essential role of neural Wiskott-Aldrich syndrome protein in podosome formation and degradation of extracellular matrix in src-transformed fibroblasts. *Cancer Res.* **62,** 669–674 (2002).
11. Rottiers, P. *et al.* TGFβ-induced endothelial podosomes mediate basement membrane collagen degradation in arterial vessels. *J. Cell Sci.* **122,** 4311–4318 (2009).
12. Varon, C. *et al.* Transforming growth factor beta induces rosettes of podosomes in primary aortic endothelial cells. *Mol. Cell. Biol.* **26,** 3582–3594 (2006).
13. Pan, Y. R., Chen, C. L. & Chen, H. C. FAK is required for the assembly of podosome rosettes. *J. Cell Biol.* **195,** 113–129 (2011).
14. Riedl, J. *et al.* Lifeact: a versatile marker to visualize F-actin. *Nat. Methods* **5,** 605–607 (2008).
15. Buccione, R., Orth, J. D. & McNiven, M. A. Foot and mouth: podosomes, invadopodia and circular dorsal ruffles. *Nat. Rev. Mol. Cell Biol.* **5,** 647–657 (2004).
16. Murphy, D. A. & Courtneidge, S. A. The 'ins' and 'outs' of podosomes and invadopodia: characteristics, formation and function. *Nat. Rev. Mol. Cell Biol.* **12,** 413–426 (2011).
17. Prewett, M. *et al.* Antivascular endothelial growth factor receptor (fetal liver kinase 1) monoclonal antibody inhibits tumor angiogenesis and growth of several mouse and human tumors. *Cancer Res.* **59,** 5209–5218 (1999).
18. Couffinhal, T. *et al.* Mouse model of angiogenesis. *Am. J. Pathol.* **152,** 1667–1679 (1998).
19. Bouvard, C. *et al.* Tie2-dependent knockout of α6 integrin subunit in mice reduces post-ischaemic angiogenesis. *Cardiovasc. Res.* **95,** 39–47 (2012).
20. Herbst, R. S., Onn, A. & Sandler, A. Angiogenesis and lung cancer: prognostic and therapeutic implications. *J. Clin. Oncol.* **23,** 3243–3256 (2005).
21. Hadler-Olsen, E. *et al.* Gelatin *in situ* zymography on fixed, paraffin-embedded tissue: zinc and ethanol fixation preserve enzyme activity. *J. Histochem. Cytochem.* **58,** 29–39 (2010).
22. Hanahan, D. Heritable formation of pancreatic β-cell tumours in transgenic mice expressing recombinant insulin/simian virus 40 oncogenes. *Nature* **315,** 115–122 (1985).
23. Block, M. R. *et al.* Podosome-type adhesions and focal adhesions, so alike yet so different. *Eur. J. Cell Biol.* **87,** 491–506 (2008).
24. Destaing, O. *et al.* β1A integrin is a master regulator of invadosome organization and function. *Mol. Biol. Cell* **21,** 4108–4119 (2010).
25. Schmidt, S. *et al.* Kindlin-3-mediated signaling from multiple integrin classes is required for osteoclast-mediated bone resorption. *J. Cell Biol.* **192,** 883–897 (2011).
26. Primo, L. *et al.* Increased expression of α6 integrin in endothelial cells unveils a proangiogenic role for basement membrane. *Cancer Res.* **70,** 5759–5769 (2010).
27. Lee, T. H. *et al.* Integrin regulation by vascular endothelial growth factor in human brain microvascular endothelial cells: role of $\alpha_6\beta_1$ integrin in angiogenesis. *J. Biol. Chem.* **281,** 40450–40460 (2006).
28. Thyboll, J. *et al.* Deletion of the laminin α4 chain leads to impaired microvessel maturation. *Mol. Cell Biol.* **22,** 1194–1202 (2002).
29. Zhou, Z. *et al.* Deletion of laminin-8 results in increased tumor neovascularization and metastasis in mice. *Cancer Res.* **64,** 4059–4063 (2004).
30. Ezratty, E. J., Partridge, M. A. & Gundersen, G. G. Microtubule-induced focal adhesion disassembly is mediated by dynamin and focal adhesion kinase. *Nat. Cell Biol.* **7,** 581–590 (2005).
31. Seano, G. *et al.* Modeling human tumor angiogenesis in a three-dimensional culture system. *Blood* **121,** e129–e137 (2013).
32. Schmidt, M. *et al.* EGFL7 regulates the collective migration of endothelial cells by restricting their spatial distribution. *Development* **134,** 2913–2923 (2007).
33. Riedl, J. *et al.* Lifeact mice for studying F-actin dynamics. *Nat. Methods* **7,** 168–169 (2010).
34. Magnussen, A. *et al.* Rapid access of antibodies to $\alpha_5\beta_1$ integrin overexpressed on the luminal surface of tumor blood vessels. *Cancer Res.* **65,** 2712–2721 (2005).
35. Eble, J. A. & Niland, S. The extracellular matrix of blood vessels. *Curr. Pharm. Des.* **15,** 1385–1400 (2009).
36. Yousif, L. F., Di Russo, J. & Sorokin, L. Laminin isoforms in endothelial and perivascular basement membranes. *Cell Adhes. Migr.* **7,** 101–110 (2013).
37. De Smet, F., Segura, I., De Bock, K., Hohensinner, P. J. & Carmeliet, P. Mechanisms of vessel branching: filopodia on endothelial tip cells lead the way. *Arterioscler. Thromb. Vasc. Biol.* **29,** 639–649 (2009).
38. Hagedorn, E. J. *et al.* Integrin acts upstream of netrin signaling to regulate formation of the anchor cell's invasive membrane in C. elegans. *Dev. Cell* **17,** 187–198 (2009).
39. Iivanainen, A. *et al.* Primary structure, developmental expression, and immunolocalization of the murine laminin α4 chain. *J. Biol. Chem.* **272,** 27862–27868 (1997).
40. Patton, B. L., Miner, J. H., Chiu, A. Y. & Sanes, J. R. Distribution and function of laminins in the neuromuscular system of developing, adult, and mutant mice. *J. Cell Biol.* **139,** 1507–1521 (1997).
41. Chan, K. T., Cortesio, C. L. & Huttenlocher, A. FAK alters invadopodia and focal adhesion composition and dynamics to regulate breast cancer invasion. *J. Cell Biol.* **185,** 357–370 (2009).
42. Mazzone, M. *et al.* Heterozygous deficiency of PHD2 restores tumor oxygenation and inhibits metastasis via endothelial normalization. *Cell* **136,** 839–851 (2009).
43. Jain, R. K. Normalizing tumor microenvironment to treat cancer: bench to bedside to biomarkers. *J. Clin. Oncol.* **31,** 2205–2218 (2013).
44. Jain, R. K. Normalization of tumor vasculature: an emerging concept in antiangiogenic therapy. *Science* **307,** 58–62 (2005).
45. Stenzel, D. *et al.* Endothelial basement membrane limits tip cell formation by inducing Dll4/Notch signalling *in vivo*. *EMBO Rep.* **12,** 1135–1143 (2011).

© 2014 Macmillan Publishers Limited. All rights reserved.

DOI: 10.1038/ncb3036

METHODS

Cell culture and reagents. Human umbilical vein endothelial cells (ECs) were isolated from umbilical cord vein, characterized and grown as previously described[46]. In all experiments, ECs were used between passages two and five. To overcome the intrinsic biological variability of ECs, all data are shown as the mean of three independent experiments performed with a mix of ECs from three different umbilical cords.

293T (ATCC CRL-11268), B16F10 (ATCC CRL-6475) and HeLa (ATCC CCL-2) cell lines were obtained from the American Type Culture Collection and maintained as frozen stock. All experiments were performed on cell lines that had been passaged for <6 months after thaw.

Rat monoclonal function-blocking antibody against integrin α_6 (GoH3, MAB13501), aspecific rat IgGA2 antibody, VEGF-A165 and FGF-2 were obtained from R&D Systems. Function-blocking antibody against α_1 (FB12; MAB1973Z), α_2 (BHA2.1; MAB1998Z), α_4 (P1H4; MAB16983Z), α_5 (P1D6; MAB1956Z) and αv (LM609; MAB1976Z) were obtained from Millipore. Each treatment was carried out with a final concentration of 20 μg ml^{-1} of azide-free antibody. Phorbol-12-myristate-13-acetate (PMA) was provided by Calbiochem. Laminin (Sigma) was isolated from Engelbreth-Holm–Swarm murine sarcoma basement membrane. Nocodazole, primaquine, cycloheximide and porcine gelatin were obtained from Sigma-Aldrich.

***In vitro* podosome analysis.** Subconfluent ECs were cultured with M199 10% FCS for 24 h and kept with or without 30 ng ml^{-1} VEGF-A for 24 h. ECs were then trypsinized and allowed to adhere for 2 h in M199 20% FCS on glass coverslips, previously coated with 1% porcine gelatin for 1 h. Cell were starved with serum-free M199 for 1 h and then stimulated for 5–60 min with 10% FCS M199 plus 80 ng ml^{-1} of PMA. To visualize podosomes, cells were paraformaldehyde (PFA)-fixed—4% PFA in PBS—and stained with anti-cortactin antibody (4F11, 05-180, Millipore) and phalloidin. We imaged ECs using a confocal laser-scanning microscope (TCS SP5 AOBS; Leica) equipped with a ×63/1.30 HCX Plan-Apochromat oil-immersion objective. Podosome-rosette-positive cells were identified by co-localization of cortactin and F-actin in a ring-like structure. Individual-podosome-positive cells were characterized by co-localization of cortactin and F-actin in a dot-like distribution. All manual quantifications were performed in a double-blind manner.

Plasmid preparation. Lentivectors carrying short hairpin RNA (shRNA) sequences against human integrin α_6 or a scramble sequence (used as control) were purchased from the RNAi Consortium library (Sigma-Aldrich). For lentivectors carrying GFP-tagged integrin α_6 (α_6–GFP) and LifeAct–RubyFP (LifeAct–RFP), we used the In-Fusion 2.0 CF Dry-Down PCR Cloning Kit (Clonetech). Integrin α_6, cloned into the pWPXL lentiviral vector (Trono lab, http://tronolab.epfl.ch), was tagged with GFP, inserted in the C terminus. LifeAct–RubyFP (ref. 14) was provided by R. Wedlich-Söldner, Max Planck Institute of Biochemistry, Martinsried, Germany, and was inserted in the pLKO.1 lentiviral vector in the place of the puromycin resistance sequence.

Lentiviral preparation, purification and concentration. Lentiviruses were produced by calcium phosphate transfection of vector plasmids—pLKO.1 shRNAs (scramble control, TRCN0000057774 and TRCN0000057775; Sigma-Aldrich), pWPXL-ITGA6, α_6–GFP and FP-tagged LifeAct—together with packaging (pCMVdR8.74) and envelope (pMD2.G-VSVG) plasmids in 293T cells. Supernatant was collected 48 and 72 h post-transfection, filtered with 0.45 μm filters and concentrated (19,000*g* for 2 h at 20 °C). The multiplicity of infection (MOI) was determined by infecting HeLa cells, plus 8 μg ml^{-1} of Polybrene, followed by puromycin selection 24 h after the infection, and quantification of resistant cells or by flow cytometric quantification of GFP-positive cells.

Transfection and lentiviral infection of ECs. ECs were transiently transfected with pTagRFP–vinculin (FP372, Evrogen) by Lipofectamine Plus (Invitrogen) according to the manufacturer's instructions.

For stable transduction, ECs were infected for 12–24 h at 1–6 MOI plus 8 μg ml^{-1} of Polybrene and mARs for 48 h with 1 million infecting virions.

Time-lapse total internal reflection fluorescence microscopy. ECs, transfected or transduced with FP-fusion-protein constructs, were incubated at 37 °C in a 5% CO_2 humidified atmosphere on gelatin-coated glass-bottom dishes (Willco, Intracel). Time-lapse experiments were performed using a Leica DMI6000 B MC TIRF system with a ×63/1.40 NA oil-immersion objective.

Blocking antibody and synthetic drug treatment in endothelial podosome rosette formation. After 24 h of VEGF treatment, subconfluent EC were trypsinized and seeded for 2 h in M199 20% FCS on glass coverslips, previously coated with 1% porcine gelatin for 1 h. Cells were starved with serum-free M199 for 30 min and then stimulated for 30 min with 10% FCS M199 plus 80 ng ml^{-1} of PMA.

Treatments with specific anti-integrin blocking antibodies were performed during a 2-hour-adhesion process in M199 20% FCS. Each treatment was carried out with a final concentration of 20 μg ml^{-1} of azide-free antibody.

Treatments with 1.25 μg ml^{-1} (4 μM) of nocodazole, 50 μg ml^{-1} (110 μM) of primaquine or 20 μg ml^{-1} of cycloheximide (CHX) were performed during a 30-min PMA stimulation. In the case of nocodazole washout experiments, ECs were treated with nocodazole for 30 min during serum-free M199 starving, and then rinsed twice in PBS and treated with PMA for 30 min. CHX pretreatment for 2 h showed results comparable to CHX treatment during PMA stimulation.

Matrix degradation assay. FITC-conjugated gelatin from pig skin was prepared according to the manufacturer's instructions (Invitrogen). ECs were plated on glass coverslips coated with FITC–gelatin (1 mg ml^{-1}), and were then fixed and stained with phalloidin for 20 min. The regions in which 488–gelatin was degraded were analysed using ImageJ (NIH), by quantifying the percentage of fluorescence reduction in the region underling ECs in comparison with zones where adhered ECs are not present.

Cytofluorimetric analysis. ECs were trypsinized and then incubated with PBS 1% BSA plus 5 μg ml^{-1} of mouse anti-integrin α_6 monoclonal antibody (4F10; sc-53356; Santa Cruz Biotechnology), active MT1-MMP monoclonal antibody (3G4.2; MAB1767; Millipore) or mouse IgG for 30 min at 4 °C. After three washes with PBS 1% BSA, cells were incubated with 2.5 μg ml^{-1} of Alexa 488-conjugated anti-mouse antibody (Invitrogen) for 30 min. After final rinses with PBS, samples were analysed with a CyAn ADP flow cytometer (Dako Cytomation) and data were analysed with Summit 4.3 software (Dako).

Integrin α_6–GFP expression analysis in ECs. We seeded integrin α_6–GFP-infected ECs on gelatin-coated dishes, with or without laminin (final concentration 20 μg ml^{-1}) for 3 h. After 30 min with M199 10% FCS with or without PMA treatment (80 ng ml^{-1}), cells were trypsinized and samples were acquired with a CyAn ADP flow cytometer (Dako Cytomation) and data were analysed with Summit 4.3 software (Dako).

RipTag2, endothelial ITGA6 KO and *Lama4*$^{-/-}$ mice. Generation of RipTag2 mice as a model of pancreatic islet cell carcinogenesis has been previously reported[47]. RipTag2 mice were maintained in the C57Bl/6J background (Jackson Laboratory). From 12 weeks of age, all RipTag2 mice received 50% sugar food (Harlan Teklad) and 5% sugar water to relieve hypoglycaemia induced by the insulin-secreting tumours. LifeAct–EGFP mice were generated previously[33], and provided by R. Wedlich-Söldner (Max-Planck Institute of Biochemistry, Martinsried, Germany) and L. M. Machesky (Beatson Institute for Cancer Research, Glasgow, UK). Mice were housed under the approval and the institutional guidelines governing the care of laboratory mice of the University of Torino Committee on Animal Research and in compliance with the international laws and policies.

Generation of α_6 floxed mice (α_6*fl/fl-Tie2Cre*+) has been reported previously[19]. For mouse breeding, both combinations were used: α_6*fl/fl-Tie2Cre*+ (KO) male with α_6*fl/fl-Tie2Cre*− (WT) female or α_6*fl/fl-Tie2Cre*− (WT) male with α_6*fl/fl-Tie2Cre*+ (KO) female. Integrin α_6 KO female mice were fertile and we did not observe any evident differences during pregnancy or in newborn number or size, as described in ref. 19. All protocols were approved by the Regional Ethics Committee on Animal Experimentation (P2.CBV.031.07, CEEA34.CB.041.11 and CEEA34.CB.011.11) and all experiments complied with Directive 2010/63/EU of the European Parliament.

Lama4$^{-/-}$ mice were generated previously[28,29].

Melanoma tumour subcutaneous injection. One million B16F10 melanoma cells were suspended in 100 μl of PBS and injected subcutaneously into the right flank of 8-week-old α_6*fl/flTie2Cre*+ and α_6*fl/flTie2Cre*− male mice. Twelve days later the mice were anaesthetized with a single intraperitoneal injection of ketamine (80 mg kg^{-1}) and xylazine (16 mg kg^{-1}), then killed by cervical dislocation. Tumours were collected and frozen in isopentane solution cooled in liquid nitrogen before being stored at −80 °C until immunohistological analysis.

Unilateral hindlimb ischaemia. The hindlimb ischaemia experiment was performed as previously described[19,48]. Male mice aged 7–8 weeks were anaesthetized with a single intraperitoneal injection of ketamine (80 mg kg^{-1}) and xylazine (16 mg kg^{-1}). The femoral artery and vein were separated from the femoral nerve, ligated, and excised from proximal to the superficial epigastric artery to proximal to the bifurcation of the saphena and popliteal arteries. On day 14 after ischaemia induction, ischaemic and non-ischaemic gastrocnemius muscles were collected and

© 2014 Macmillan Publishers Limited. All rights reserved.

frozen slowly in isopentane solution cooled in liquid nitrogen, before being stored at −80 °C.

Human lung tumour data. Endothelial podosome rosette levels, microvessel density (MVD) and VEGF area fraction were measured in the lung tumour samples of a cohort of patients collected between 1992 and 1993 before surgical resections with the approval of the Massachusetts General Hospital Institutional Review Board and previously analysed in ref. 49. The Massachusetts General Hospital Institutional Review Board determined that our investigation did not meet the definition of 'human subjects research'. We did not obtain data through an intervention or interaction with individual subjects or identifiable private information about living individuals. The patients had a variety of pre- and post-surgical treatments and tumour stages. We analysed 11 biopsies, 3 vessels per tumour for rosette quantification and 20 different regions of interest (ROIs) per biopsy for MVD and VEGF.

Immunostaining. ECs plated on coated glass coverslips, whole-mount mouse aortic explants, whole-mount mARs or 30–50 µm cryosections of mice tumours were equilibrated in PBS, PAF-fixed and permeabilized with PBS 0.3% Triton X-100. For biopsy, samples from human patients, 10-µm-formalin-fixed paraffin-embedded (FFPE) sections were de-waxed and permeabilized with PBS 0.3% Triton-X100. Primary antibodies—mouse anti-cortactin (1:100, 4F11; 05-180; Millipore), rabbit anti-paxillin (1:100, Y113; 04-581; Millipore), goat anti-MT1-MMP (1:100, 3G4.2; MAB1767; Millipore), rabbit anti-MT1-MMP (1:150, AB53712, Abcam), mouse anti-dynamin (1:100, E-11; sc-74532; Santa Cruz Biotechnology), rabbit anti-phospho-cortactin (1:100, Tyr 421; AB3852; Millipore), mouse anti-phospho-FAK (1:80, Tyr 397; ABT135; Chemicon), mouse anti-vinculin (1:1,000, hVIN-1; V3191; Sigma-Aldrich), mouse anti-α_1 integrin (1:100, FB12; MAB1973; Millipore), mouse anti-$\alpha_2\beta_1$ integrin (1:100, BHA2.1; MAB1998; Millipore), mouse anti-α_3 integrin (1:100, P1B5; MAB1952; Millipore), mouse anti-α_4 integrin (1:100, P4C2; MAB1955; Millipore), mouse anti-α_5 integrin (1:50, P1D6; MAB1956; Millipore), mouse anti-$\alpha v\beta_3$ integrin (1:100, LM609; MAB1976; Millipore), rat anti-α_6 integrin (1:50, GoH3; MAB13501; R&D System), mouse anti-β_4 integrin (1:100, 450-11, a gift from R. Falcioni, National Cancer Institute 'Regina Elena', Rome, Italy), and rabbit anti-laminin (1:80, AB2034, Millipore)—were diluted in PBS 5% donkey serum and incubated overnight at 4 °C in a humidified chamber. Coverslips or specimens were washed with PBS and incubated for 30 min at room temperature with secondary antibodies and counterstained with Alexa488-conjugated phalloidin (Invitrogen) and 4′,6-diamidino-2-phenylindole (DAPI). Coverslips or specimens were analysed using a confocal laser-scanning microscope (TCS SP5 AOBS; Leica) equipped with a ×63/1.30 HCX Plan-Apochromat oil-immersion objective. Confocal stack images were digitally post-processed with blind deconvolution algorithms.

Endothelial podosome density in tumours. We stained tumour slices with anti-laminin (1:80, AB2034, Millipore) and anti-cortactin (4F11, 05-180, Millipore) antibody and phalloidin and performed confocal imaging with a laser-scanning microscope (TCS SP5 AOBS; Leica) equipped with a ×63/1.30 HCX Plan-Apochromat oil-immersion objective. After three-dimensional (3D) blind deconvolution algorithms, tumour vessel volumes were recognized by using laminin staining using Imaris 6.3 software (Bitplane, AG). To count endothelial podosome rosettes, several discriminating criteria were followed: endothelial podosome rosettes were identified as ring-like structures within vessels with co-staining for F-actin and cortactin, close to a region depleted in laminin staining, and with a diameter ranging between 2 and 6 µm. All manual quantifications were performed in a double-blind manner.

***In situ* zymography.** Tissue sections (RipTag2 or human lung tumours) or whole-mount mARs were fixed in acetone and immunostained as indicated. Substrate for *in situ* zymography was prepared by diluting DQ gelatin (0.1% in deionized H_2O, Invitrogen) 1:50 in a reaction buffer containing PBS 5 mM $CaCl_2$. Tissue sections or whole-mount mARs were incubated in a dark humidity chamber at 37 °C in gelatin solution for 2 h. Samples were then carefully rinsed with PBS and PFA-fixed for 10 min in the dark. To verify the contribution of metalloproteases, control slides were pre-incubated with 20 mM EDTA or protease inhibitor mix (leupeptin, aproptin and pepstatin) for 1 h. Specimens and whole-mount mARs were analysed using a confocal laser-scanning microscope (TCS SP5 AOBS; Leica) equipped with a ×40/0.95 or ×63/1.30 HCX Plan-Apochromat oil-immersion objective. Confocal stack images were digitally post-processed with deconvolution algorithms.

Immunohistochemistry on human tissues. FFPE sections (5 µm thick) were immunostained following the manufacturer's recommendations and standard protocols with antibodies against the following antigens: mouse anti-human CD31 (JC70A; 102870; Dako) and mouse anti-human VEGF (Ab-7; MS-1467-P0; Thermo Scientific). Sections were visualized by the avidin–biotin complex immunoperoxidase method, observed with a bright-field microscope and photographed. MVD and VEGF-positive area were estimated in 20 ROIs of the tumour on CD31- or VEGF-stained sections using a customized analysis with ImageJ (NIH).

Intravenous injection of antibody and detection. Rapid accessibility of antibody was analysed as previously described[26,50]. 25 µg of anti-α_6 (GoH3, R&D) or nonspecific IgG, diluted to 125 µl final volume with 0.9% NaCl, were injected through the tail vein. Antibodies were allowed to circulate for 10 min and the tissues were fixed by vascular perfusion. The chest was opened rapidly, and the vasculature perfused for 3 min with PFA fixative from a cannula inserted into the aorta through an incision in the left ventricle. The right atrium was incised to provide an exit for the fixative. After the perfusion, tissues were removed, stored and obtained as OCT-embedded sections. The localization of antibodies was detected by incubating sections with Alexa-647 goat anti-rat antibody, phalloidin and anti-cortactin antibody. Confocal stack images were post-processed with blind deconvolution algorithms with Autodeblur (Media Cybernetics) and ImageJ (NIH).

Therapeutic antibody treatment. The therapeutic antibody treatment was performed in RipTag2 mice as previously described[26]. In brief, the dosage regimen used was 0.125 mg of anti-α_6 integrin antibody (GoH3, R&D) per mouse through tail vein injection. Antibody treatment started when mice reached the age of 9 weeks and continued for 15 days. Control animals were treated with purified rat IgG2A (R&D) at a dose of 0.125 mg per mouse every 2 days for 2 weeks. Cohorts of 6 mice were treated for each arm of the trial study.

Vascular branching index in tumours. The vessel branching index (also 'vessel branching incidence') is the number of manually counted branching points/vascular volume and is independent of the vascularization rate. We stained tumour slices with anti-laminin (1:80, AB2034, Millipore) or anti-CD31 (JC70A; 102870; Dako) antibody and analysed them using a confocal laser-scanning microscope (TCS SP5 AOBS; Leica) equipped with a ×20/1.40 HCX Plan-Apochromat oil-immersion objective. After maximum projection of 30-µm-slices, we manually counted branching points and divided them by a given vessel volume as described above. All manual quantifications were performed in a double-blind manner.

***Ex vivo* podosome stimulation in aortic explants.** Aortas were explanted as previously described[26]. After isolation from fibro-adipose tissue, aortae were cut along their long axis and then sectioned in 1 mm^2 squares and then incubated for 24 h in serum-free medium with antibiotics. Aortic segments were incubated for 48 h in M199 10% FCS plus antibiotics with or without 30 ng ml^{-1} of VEGF-A. In the case of knockdown experiments media were supplied with Polybrene and lentiviral supernatants.

To visualize podosome-positive cells, we PFA-fixed aortic explants and stained them with anti-cortactin (4F11, 05-180, Millipore) antibody and phalloidin and imaged them using a confocal laser-scanning microscope (TCS SP5 AOBS; Leica) equipped with a ×40/0.95 HCX Plan-Apochromat oil-immersion objective. After 3D blind deconvolution algorithms (ImageJ plugins), podosome-positive cells in the endothelial layer were recognized by identifying regions of co-localization of cortactin and F-actin in ring-like structures in the endothelial layer. The endothelial layer was easily identified as ECs are not as highly stained by phalloidin as smooth muscle cells (SMCs); the endothelial layer and the SMC layer are divided by a highly autofluorescing layer of elastin; moreover, the circularity of nuclei allowed to distinguish ECs from SMCs because endothelial nuclei are circular and not elongated[11]. These criteria were previously described[11] and are summarized in Supplementary Fig. 1d. All manual quantifications were performed in a double-blind manner.

Mouse aortic ring angiogenesis assay. The mouse aortic ring (mAR) assay was performed as previously described[26,31] with the following with modifications. After explant, mARs were incubated for 2 days in serum-free medium. Aortic explants were then kept in place on glass-bottom dishes (Willco, Intracel) with a drop of 20 µl of type-I collagen gel (from rat tail, Roche) and covered with Endothelial Basal Medium (EBM, Clonetics) 5% FCS with VEGF-A (20 ng/ml, R&D) and FGF-2 (10 ng ml^{-1}, R&D).

Time-lapse analysis of mAR model. LifeAct–EGFP, endothelial α_6 null and *Lama4*$^{-/-}$ mARs were embedded in type-I collagen gel, stimulated as described previously and kept at 37 °C in a 5% CO_2 humidified atmosphere for 24–72 h on glass-bottom dishes.

LifeAct–EGFP, endothelial α_6 null or *Lama4*$^{-/-}$ mARs were imaged with a ×20/0.75 dry objective (Leica Microsystems) with an inverted photomicroscope (DM IRB HC; Leica Microsystems) in phase-contrast or epifluorescence.

© 2014 Macmillan Publishers Limited. All rights reserved.

DOI: 10.1038/ncb3036

LifeAct–EGFP mARs were imaged with a ×20/0.50 dry objective (Leica Microsystems) with a multiphoton microscope Leica TCSII SP5. *Z* stacks were acquired at 512 × 512 resolution, scan speed of 400 Hz, and 1 µm *z*-step size.

To investigate the relation between endothelial podosome rosettes and lateral sprouting, we analysed 8 lateral protrusion events from 3 different mARs. We measured the time of persistence and diameter of ring-like structures. Data obtained in LifeAct–GFP mARs were corroborated by the quantification of rosettes in fixed confocal sections of mARs identified by co-staining of cortactin (4F11, 05-180, Millipore) and F-actin. Rates of rosettes per unit length and time were calculated by knowing the duration of rosettes and assuming a uniform density over every branch of the mAR. Lateral sprouting in mARs was instead quantified in live bright-field movies, where we identified protrusions emerging from pre-existing branches and either retracting or developing into full secondary branches.

Integrin α_6 membrane localization in mARs. After 10 days of culture, live mARs were treated with the rat anti-antibody GoH3 (0.2 µg ml^{-1} MAB13501; R&D System) for 1 h and then PFA-fixed. The localization of the anti-a6 antibody (GoH3) was detected by whole-mount incubation with Alexa-647-conjugated goat anti-rat antibody, anti-cortactin (4F11, 05-180, Millipore) antibody, phalloidin and DAPI. We quantified the anti-α_6 antibody in cells with or without endothelial rosettes by using phalloidin and DAPI staining to distinguish the cell edges and phalloidin and cortactin for podosome rosettes (shown in Supplementary Fig. 7e). Confocal stacks of images were quantified using ImageJ (NIH).

Image analysis. Immunostained cryosections of mouse tumours or whole-mounted mARs were imaged using a confocal laser-scanning microscope (TCS SP5 AOBS; Leica) equipped with a ×40/0.95 (*z*-step = 0.4 µm) or ×63/1.30 HCX Plan-Apochromat oil-immersion objective (*z*-step = 0.3 µm). To increase the signal to noise ratio, confocal images were obtained by using a high line average and a low scan speed.

To reduce optical distortions, images were filtered with blind deconvolution algorithms by means of Autodeblur (Media Cybernetics). We applied 5 iterations for light microscopy, 10 for confocal stacks, and 3 for multiphoton 4D analysis. Podosome rosettes were identified in deconvoluted stacks and checked, *a posteriori*, in each raw stack.

For ease of visualization, we reconstructed the 3D geometry of confocal stacks by isosurface rendering using Imaris 6.3 (Bitplane, AG). Briefly, each channel was binarized with a threshold level chosen automatically by the software.

Fluorescence image quantification. Fluorescence intensity quantification was performed using Leica Confocal Software (Leica), ImageJ (NIH) or Imaris 6.3 (Bitplane, AG). Image acquisition was performed maintaining the same laser power, gain and offset settings. In the case of *in vitro* experiments, we analysed 10 different cells for each experimental point, in three independent experiments. Integrin α_6 localization in podosome rosettes was detected as mean fluorescence in podosome ROIs. Podosome ROIs were manually selected by using co-localization of cortactin and phalloidin staining.

In the case of vBM fluorescence quantification in proximity of endothelial podosome rosettes, we analysed 5 different fields for each mouse. After 3D blind deconvolution algorithms, tumour vessel volumes were recognized by using isosurface of vBM staining. vBM was detected as laminin staining. Volumes of vBM were subdivided in 1,000-µm^3-volumes. The volumes of vBM were then classified in vBM volumes with or without endothelial rosettes. Mean fluorescence of laminin staining in vessel volumes was quantified by Imaris 6.3 (Bitplane, AG).

Statistical analysis. No statistical method was used to predetermine sample size, but the sample size was conceived to obtain a 95% confidence level and a confidence interval of 5%, which were verified *a posteriori* once the experiment was performed. For cells and aortic explants, we used the experiments in Fig. 1 to set the maximum (VEGF-A stimulation) and the minimum (unstimulated) for the following experiments. The animal numbers for anti-α_6 treatments and for integrin α_6 null mice experiments are based on similar experiments in the past[19,26]. The investigators were not blinded during the treatments, but they were blinded for all image analyses and manual quantifications. The experiments were not randomized.

Data are presented as means ± standard error (s.e.m.) of three independent experiments. For *in vitro* assays, each experiment was performed with a mix of ECs from three different umbilical cords. For digital quantification of fluorescence in specific ROIs, we measured 6 fields per experimental point in three independent experiments. For *in vivo* studies, cohorts of 6 mice were treated for each arm of the anti-α_6 antibody treatment study in RipTag2 mice, cohorts of 7 mice were analysed for each arm of the B16F10 tumours in α_6 null mice and cohorts of 3 mice for ischaemic experiments in α_6 null mice. For human sample analysis, we studied 11 biopsies, three different vessels per biopsy and the measurement of 20 ROIs per slide for MVD and VEGF.

Prism (GraphPad Software) was used for analysis. Statistical analyses were performed using unpaired *t*-tests or, when more than two groups were assessed, by ANOVA followed by Bonferroni-adjusted *post hoc t*-tests. *F*-tests were used to determine whether groups had equal variance; if equality was not established unpaired *t*-tests with Welch's correction were performed. A D'Agostino–Pearson test was used to assess normality. A Mann–Whitney test was used when normality was not achieved. A Pearson test was used for correlation analyses in human tissues because all three sets (rosette densities, MVD and VEGF areas) passed the normality test. Statistical significance was achieved when *P* was less than 0.05.

For representative images, we repeated the experiments multiple times: Fig. 1a (10 cells), Fig. 1d (5 cells), Fig. 1e (5 aortic explants), Fig. 2a (5 fields per mouse in 3 mice, 3 fields per biopsy for a total of 33 images), Fig. 2b (2 fields per mouse in 3 mice), Fig. 3f (6 aortic explants), Fig. 5a (5 different cells), Fig. 6a (3 mARs), Fig. 6b (3 mARs), Fig. 6c (4 sprouts), Fig. 6d (8 lateral sprouts), Fig. 7a (2 fields per mouse in 3 mice). Supplementary Fig. 1a (5 cells per podosomal marker), Supplementary Fig. 1b (3 cells), Supplementary Fig. 1e (5 aortic explants), Supplementary Fig. 2b (2 fields), Supplementary Fig. 2c (9 fields), Supplementary Fig. 2e (2 fields), Supplementary Fig. 2f (3 fields in 2 different biopsies), Supplementary Fig. 3a (5 fields per mouse in 3 mice, 3 fields per biopsy for a total of 33 images), Supplementary Fig. 3b (2 fields), Supplementary Fig. 3c (20 fields per slide for MVD and VEGF), Supplementary Fig. 4a (at least 3 cells per marker), Supplementary Fig. 5b (2 cells), Supplementary Fig. 5c (6 aortic explants), Supplementary Fig. 6e (3 cells), Supplementary Fig. 7a (2 mARs), Supplementary Fig. 7b (2 mARs), Supplementary Fig. 7c (3 mARs), Supplementary Fig. 7c (3 mARs), Supplementary Fig. 7e (12 fields), Supplementary Fig. 7f (2 mARs), Supplementary Fig. 7i (2 fields in 2 different mice), Supplementary Fig. 7l (3 fields in 2 different biopsies).

46. Bussolino, F. *et al.* Hepatocyte growth factor is a potent angiogenic factor which stimulates endothelial cell motility and growth. *J. Cell Biol.* **119,** 629–641 (1992).
47. Hanahan, D. Heritable formation of pancreatic beta-cell tumours in transgenic mice expressing recombinant insulin/simian virus 40 oncogenes. *Nature* **315,** 115–122 (1985).
48. Couffinhal, T. *et al.* Mouse model of angiogenesis. *Am. J. Pathol.* **152,** 1667–1679 (1998).
49. Padera, T. P. *et al.* Lymphatic metastasis in the absence of functional intratumor lymphatics. *Science* **296,** 1883–1886 (2002).
50. Magnussen, A. *et al.* Rapid access of antibodies to α5β1 integrin overexpressed on the luminal surface of tumor blood vessels. *Cancer Res.* **65,** 2712–2721 (2005).

© 2014 Macmillan Publishers Limited. All rights reserved.

DOI: 10.1038/ncb3036

nature cell biology

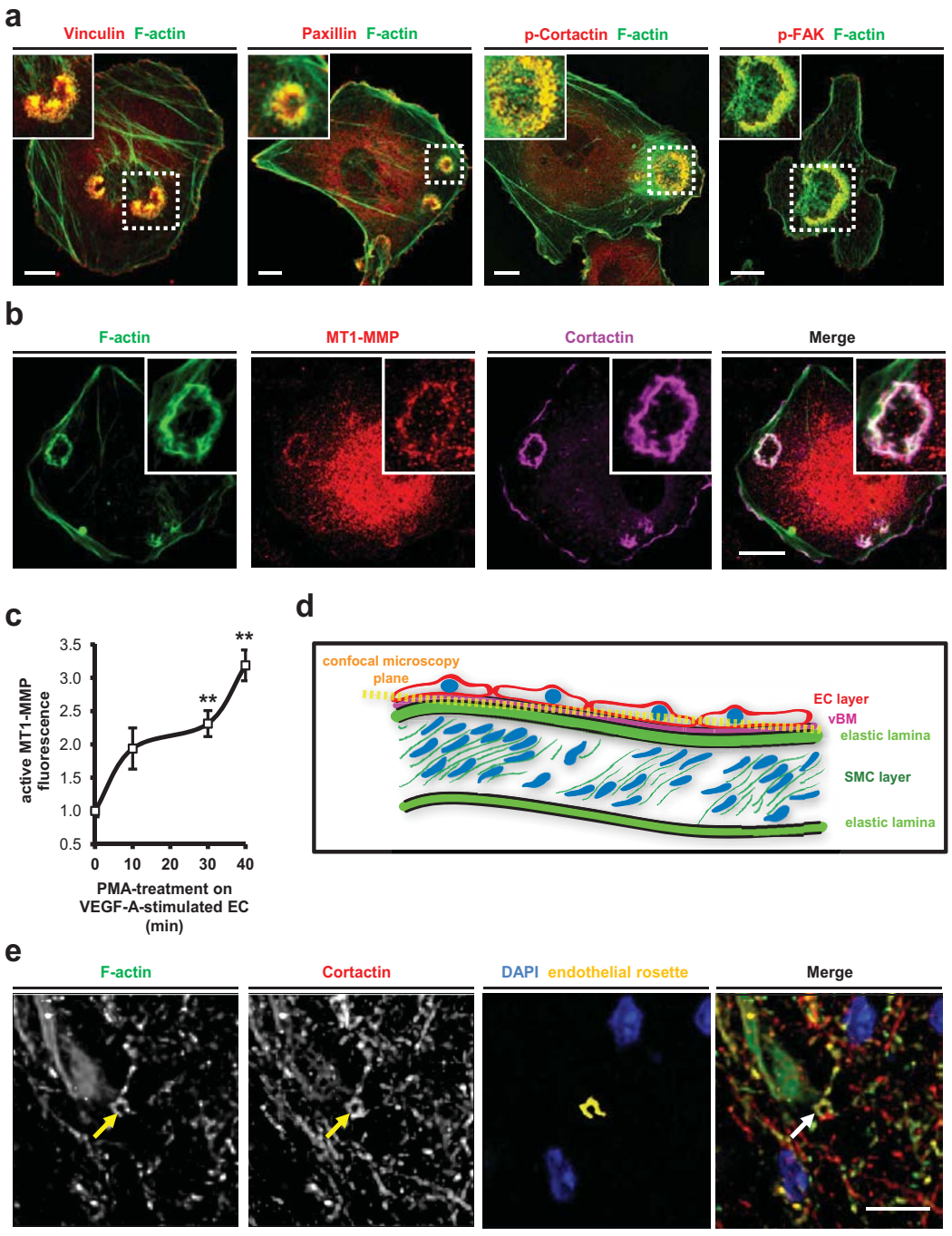

Supplementary Figure 1 Endothelial podosome rosettes in cultured EC and aortic explants. (**a-b**) Immunostained representative VEGF-A-stimulated EC treated with PMA for 30 min. Scale bar: 10 µm. (**c**) Cytofluorimetric analysis of membrane MT1-MMP localization. EC treated with PMA for the indicated time. Normalized mean ± SEM of n = 3 independent experiments in which 8×10^4 cells were analyzed per experimental point. (**, P < 0.01 versus *T=0*.) Statistical significance was calculated using paired nonparametric Wilconox test. (**d**) Schematic representation of mouse aortic explant micro-anatomy. Endothelial cells (EC) are characterized by large round nuclei and vascular smooth muscle cells (SMC) by thin and elongated nuclei. Along the z-axis, the two cell types were seen separated by the top elastic lamina. Yellow dotted line, schematization of the *z* plane of microscopic analysis of endothelial rosettes. (**e**) Immunostaining of a representative 48 h VEGF-A-stimulated aortic explant. In yellow, 3D reconstruction of the co-localization channel in podosome rosette. Individual channel images from Fig. 1e. Scale bar: 20 µm.

© 2014 Macmillan Publishers Limited. All rights reserved.

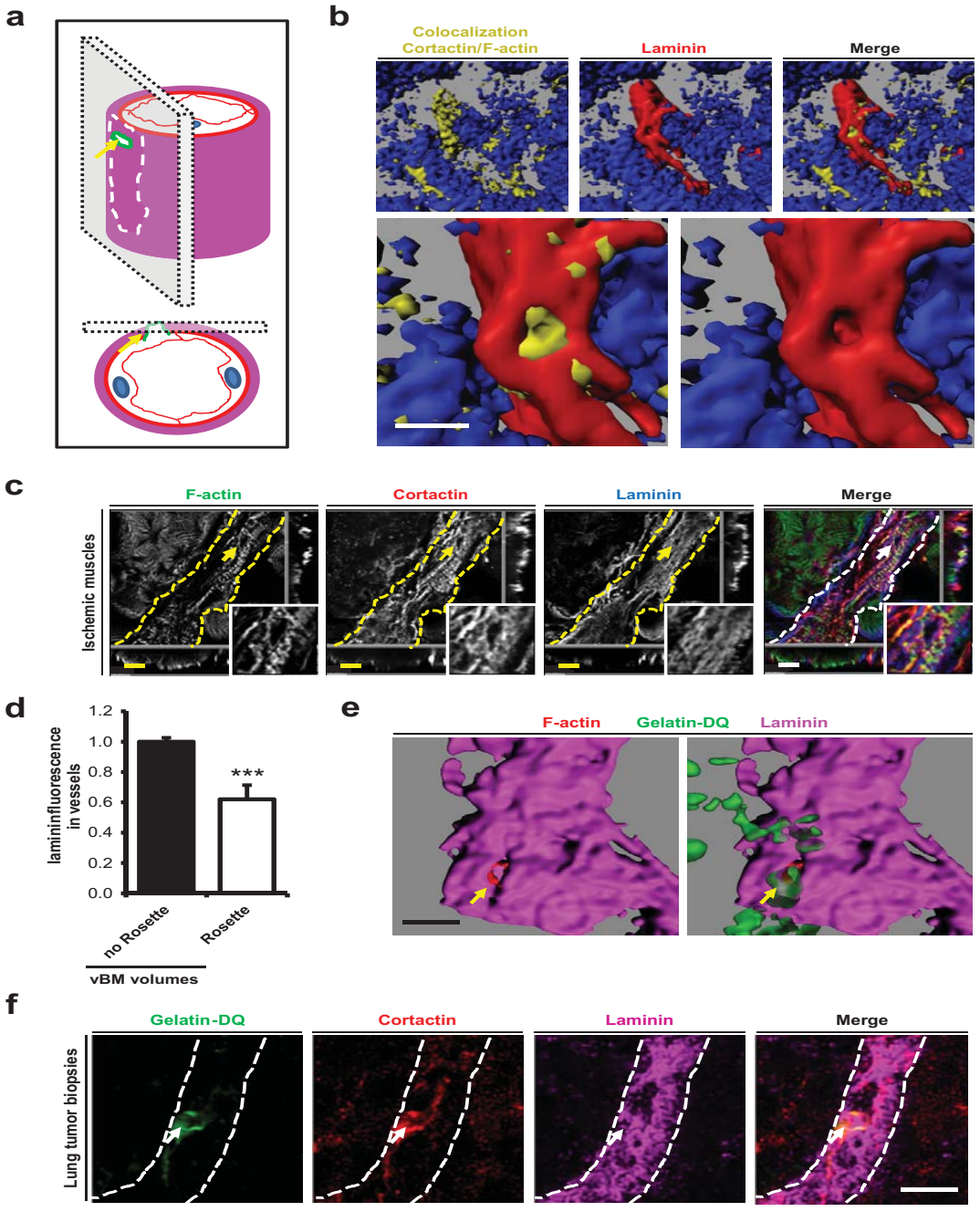

Supplementary Figure 2 3D rendering of endothelial podosome rosettes in RipTag2 tumour and ischaemic vessels. (**a**) Schematic representation of endothelial tumoural rosettes detection. Endothelial cells (EC) are delimited by red line while vBM is colored in magenta, in green there is the schematization of endothelial tumoural rosettes visualized as shown in Fig. 2a. Yellow arrows indicate the rosettes. (**b**) 3D reconstruction of a representative endothelial rosette in RipTag2 tumours. Isosurface of vBM – detected as laminin staining – was coloured in red, endothelial rosettes – F-actin/cortactin co-localization – in yellow and nuclear staining in blue. Scale bar: 5 µm. (**c**) Confocal imaging stacks of representative vessels in hindlimb ischaemia experiment on gastrocnemius muscles. *Xyz*-section of immunostaining for primary Abs as indicated. Vessels are delimited by white dotted lines; white arrows indicate podosome-rosettes. Scale bar: 10 µm. (**d**) vBM quantification in different regions of tumour vessels in RipTag2 tumours. vBM was detected as laminin staining. vBM volumes were subdivided in 1000-µm^3-volumes. Therefore, the sub-volumes of vBM were classified in vBM volumes without endothelial rosettes (*no rosette vBM volumes*) and vBM volumes with endothelial rosettes (*rosette vBM volumes.*) Normalized mean ± SEM of n = 420 subvolumes of vBM from 5 fields per mouse for a total of 3 mice per treatment group. (***, $P < 0.001$ versus *no rosette vBM volumes.*) Statistical significance was calculated using unpaired nonparametric Mann-Whitney test. (**e**) 3D reconstruction of *in situ* zymography in a representative endothelial rosette of RipTag2 tumours. After deconvolution, isosurface of vBM – detected as laminin staining – was coloured in magenta, F-actin in red and Gelatin-DQ – indication of gelatin degradation – in green. Scale bar: 10 µm. (**f**) *In situ* zymography in lung tumours from patients. Staining for primary Abs as indicated and Gelatin-DQ (dye-quenched), *i.e.* degradated gelatin. Vessel is delimited by white dotted lines; white arrows indicate podosome-rosettes. Scale bar: 10 µm.

© 2014 Macmillan Publishers Limited. All rights reserved.

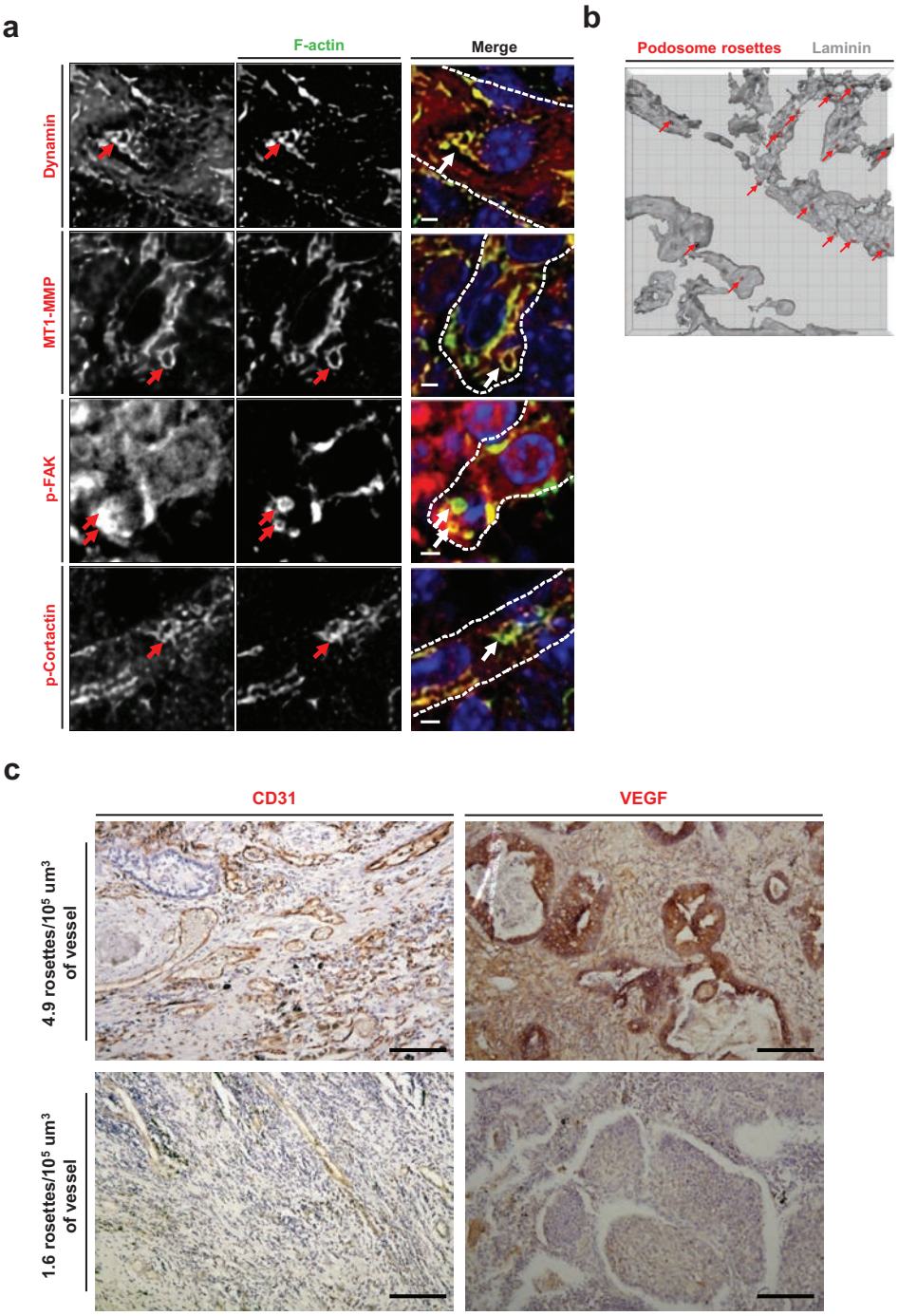

Supplementary Figure 3 Endothelial podosome markers and endothelial density in tumours vessels. (**a**) Confocal images of representative vessels in angiogenic islets of RipTag2 mice. *Xyz*-section of immunostaining for primary Abs as indicated and nuclear-stained by DAPI (blue). Vessels are delimited by white dotted lines; white arrows indicate podosome-rosettes. Scale bar: 3 µm. (**b**) 3D isosurface rendering of tumour vessels in a 12-µm-thick slice of a representative RipTag2 angiogenic islet. Vessels (gray) detected with laminin staining and podosome-rosettes (red) recognized with co-localization of F-actin/cortactin staining. Red arrows indicate podosome-rosettes. Tickmarks on axis: 10 µm. (**c**) Representative micrograph images of CD31 and VEGF staining in biopsy samples of lung tumours. Scale bar: 50 µm. Quantifications and correlations in Fig. 2d.

© 2014 Macmillan Publishers Limited. All rights reserved.

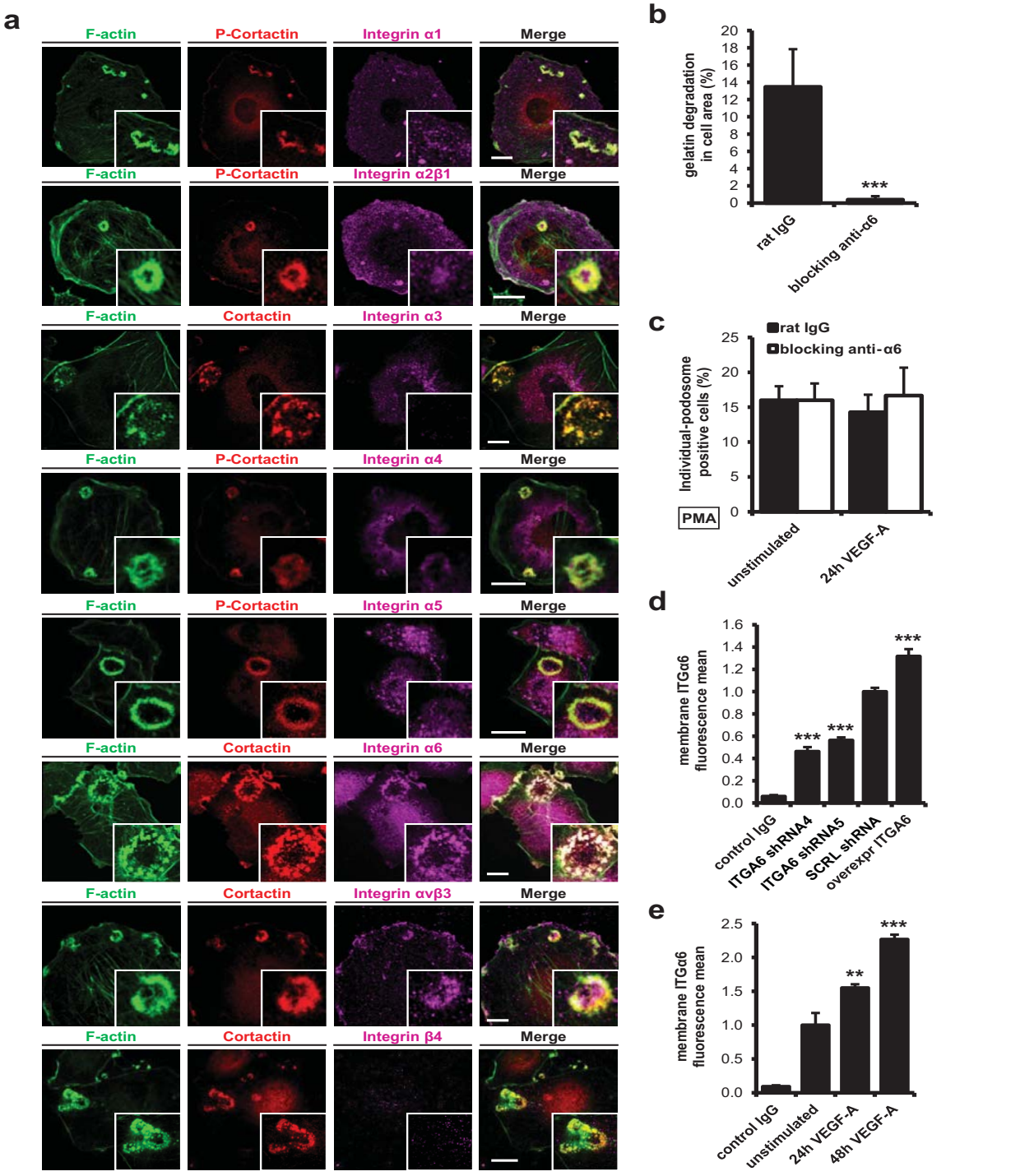

Supplementary Figure 4 Integrin recruitment in endothelial podosome rosettes. (**a**) Confocal images of representative VEGF-stimulated EC, PMA-treated for 30 min. Inset, of the podosome-rosettes. Scale bar: 20 μm. (**b**) Gelatin degradation assay on EC treated with rat IgG or anti-α6 blocking Ab after 1 hour of stimulation with PMA. Mean ± SEM of n = 10 cells from 3 independent experiments (***, P < 0.001 versus *Rat IgG*.) Statistical significance was calculated using unpaired nonparametric Mann-Whitney test. (**c**) Graph shows the percentages of individual podosome positive EC, stimulated as indicated and treated with rat IgG or anti-α6 blocking Ab. Mean ± SEM of n = 3 independent experiments in which 250 total cells were analyzed cells per experimental point. (**d**) Cytofluorimetric analysis of membrane integrin α6 localization. EC were transduced with shRNA scramble (*SCRL shRNA*) or against integrin α6 (*ITGA6 shRNA4* and *shRNA5*). Mean ± SEM of n = 3 independent experiments (***, P < 0.001 versus *shSCRL*.) Statistical significance was calculated using one-way ANOVA test followed by Bonferroni adjusted post-hoc t-tests. (**e**) Cytofluorimetric analysis of membrane integrin α6 localization. EC were incubated for 24 h in M199 10% FCS (*unstimulated*) or in M199 10% FCS plus 30 ng/ml of VEGF-A (*24 h VEGF-A*) or for 48 h in M199 10% FCS plus 30 ng/ml of VEGF-A (*48 h VEGF-A*). Mean ± SEM of n = 3 independent experiments. (**, P < 0.01 versus *unstimulated*; ***, P < 0.001.) Statistical significance was calculated using one-way ANOVA test followed by Bonferroni adjusted post-hoc t-tests.

© 2014 Macmillan Publishers Limited. All rights reserved.

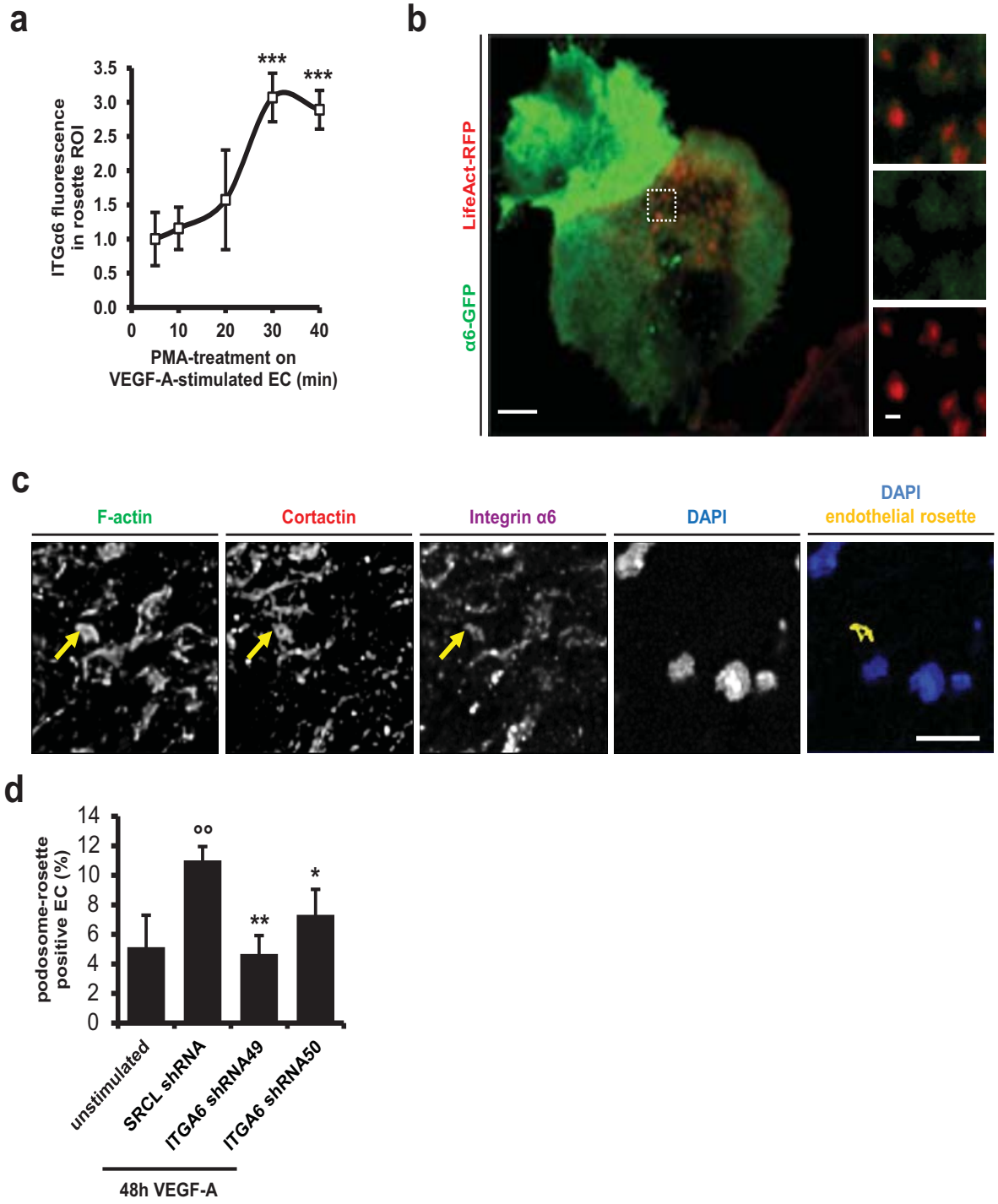

Supplementary Figure 5 Integrin α6 recruitment in endothelial podosomes and integrin α6 silencing in aortic explants. (**a**) Integrin α6 fluorescence quantification in rosettes regions. Rosettes regions were manually selected using co-localization of cortactin and F-actin staining. Mean ± SEM of n = 3 independent experiments in which 30 total cells were analyzed cells per experimental point. (***, P < 0.001 versus *T=0*.) Statistical significance was calculated using paired nonparametric Wilconox test. (**b**) TIRF microscopy of LifeAct-RFP (red) and α6-GFP (green) localization in EC treated with PMA for 15 min. EC were seeded on gelatin-coated glass-bottom dishes. The complete sequence of time-lapse TIRF microscopy is shown in Supplementary Video 2. Scale bar: 20 µm. Zoom of white dotted square is shown in the lower panels. Scale bar: 1 µm. (**c**) Endothelial layer of a 48 h VEGF-A-stimulated aortic explant from Fig. 3f. In yellow, 3D reconstruction of the co-localization channel in podosome rosette. Scale bar: 20 µm. (**d**) Aortic explants were incubated for 48 hours in M199 10% FCS (*unstimulated*) or M199 10% FCS with 30 ng/ml of VEGF-A (*48 h VEGF-A*) plus lentiviruses carrying scramble shRNA (*SCRL shRNA*) and shRNA targeting murine ITGA6 (*shRNA48 and shRNA50*). Graph shows the percentage (%) of podosome-rosettes positive in the endothelial layer of aortic explants, treated and transduced as indicated. Mean ± SEM of n = 3 independent experiments in which 340 total nuclei were analyzed cells per experimental point. (°°, P < 0.01 versus *unstimulated*; *, P < 0.05 versus *SCRL shRNA*; **, P < 0.01 versus *SCRL shRNA*.) Statistical significance was calculated using one-way ANOVA test followed by Bonferroni adjusted post-hoc t-tests.

© 2014 Macmillan Publishers Limited. All rights reserved.

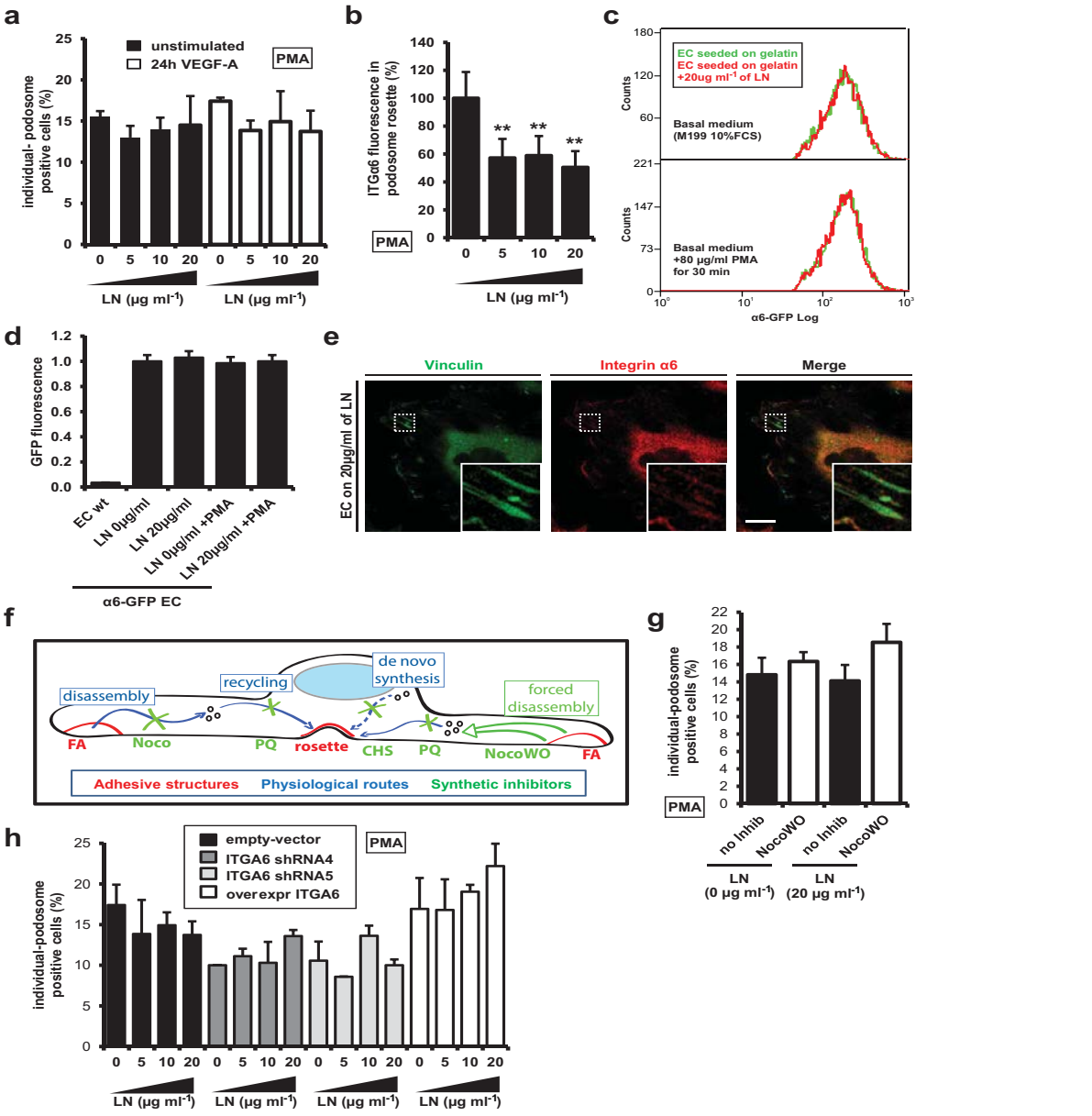

Supplementary Figure 6 Laminin effects on individual podosomes. (**a**) Graph shows the percentages of individual podosome positive EC, stimulated as indicated and seeded on gelatin coated-coverslips with addition of laminin. Percentages of podosome-rosette positive cells in Fig. 4a. Mean ± SEM of n = 3 independent experiments in which 260 total cells were analyzed cells per experimental point. (**b**) Integrin α6 fluorescence quantification in rosettes regions of VEGF-A-stimulated EC. Rosettes ROI were manually selected using the co-localization of cortactin and F-actin staining. Normalized mean ± SEM of n = 3 independent experiments in which 30 cells were quantified per experimental point. (**, $P < 0.01$ versus *LN=0*.) Statistical significance was calculated using one-way ANOVA test followed by Bonferroni adjusted post-hoc t-tests. (**c-d**) Degradation of α6-GFP in PMA-treated EC on laminin. Cytofluorimetric analysis of GFP fluorescence in α6-GFP-transduced EC. EC stimulated as indicated and seeded on gelatin coated-plates with indicated addition of laminin. Mean ± SEM of n = 3 independent experiments in which 10^5 cells were analyzed per experimental point. (**e**) Confocal image of a representative VEGF-stimulated EC seeded on glass-bottom dishes coated with gelatin plus 20 µg/ml of laminin for 2 hours. Inset, of focal adhesion. Scale bar: 20 µm. (**f**) Schematic representation of trafficking model accordingly data shown in Fig. 5a,b. Disassembly of focal adhesions (FA) allows to recruit structural components that are recycled in newly-formed rosettes. Nocodazole (*Noco*) blocks FA disassembly, primaquine (*PQ*) blocks integrin recycling, while *de novo* synthesis blocked by cicloheximide (*CHS*) does not modulate endothelial rosette formation. (**g**) Graph shows the percentages of podosome-rosettes positive EC, seeded on gelatin-coated with indicated laminin addition and PMA-treated with or without nocodazole washout. Percentages of podosome-rosette positive cells in Fig. 5C. Mean ± SEM of n = 3 independent experiments in which 230 cells were analyzed per experimental point. No statistical significance in the modulation of individual podosome was seen. (**h**) Graph shows the percentages of podosome-rosettes positive EC, seeded on gelatin coated-coverslips with indicated addition of laminin. EC were stable-transduced as indicated. Membrane integrin α6 levels in transduced EC are shown in Supplementary Fig. 4d. Percentages of individual-podosome positive cells in Fig. 5d. Mean ± SEM of n = 3 independent experiments in which 420 total cells were analyzed cells per experimental point. No statistical significance in the modulation of individual podosome was seen.

© 2014 Macmillan Publishers Limited. All rights reserved.

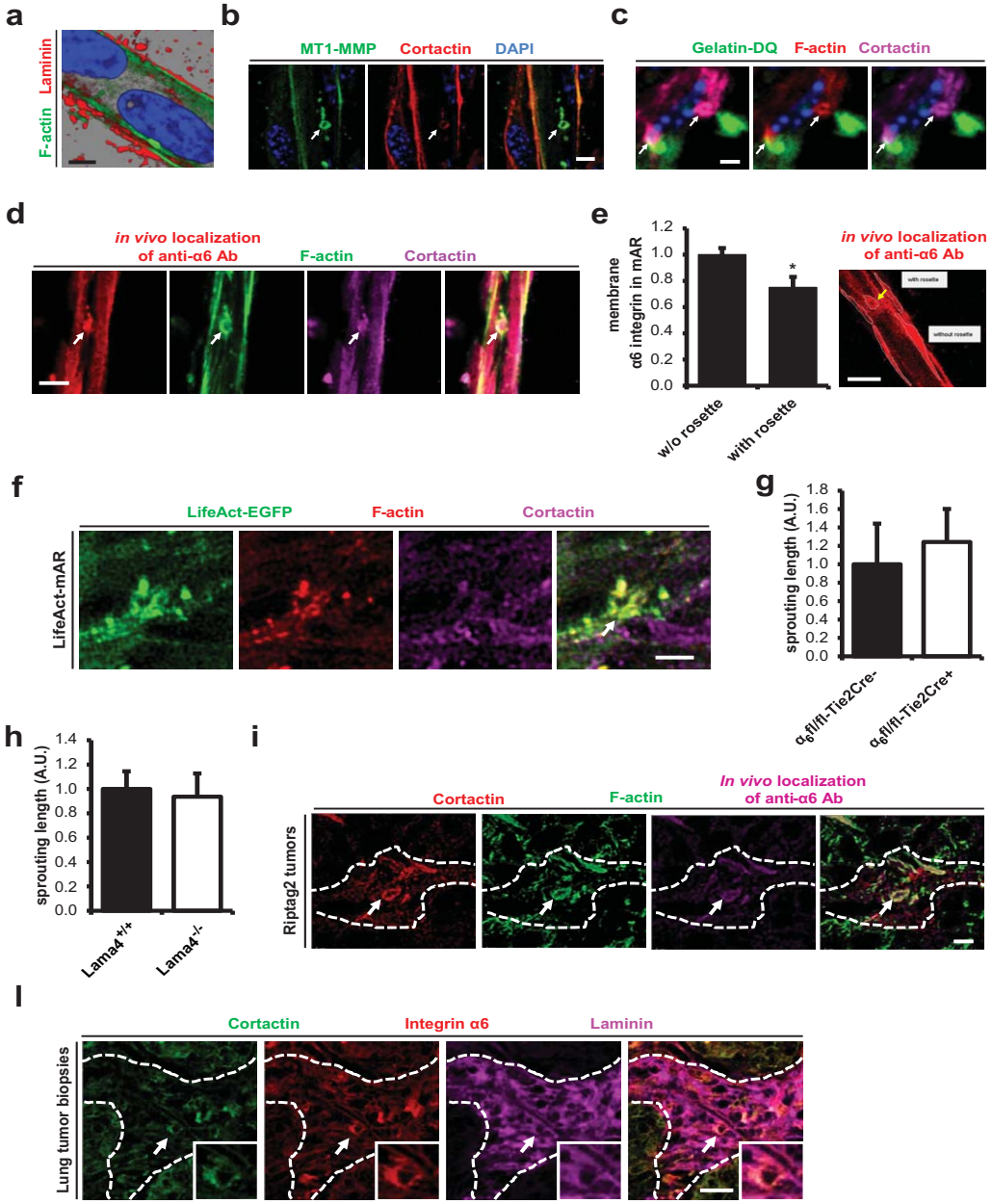

Supplementary Figure 7 Endothelial podosome rosettes in mAR and tumours. (**a**) Self-produced vBM layer – detected as laminin staining – in mAR model. Confocal images of immunostainings for primary Abs as indicated. Scale bar: 5 µm. (**b**) High-magnification confocal images of immunostaining for MT1-MMP in 7-day mAR model. White arrows indicate podosome-rosettes. Scale bar: 5 µm. (**c**) *In situ* zymography in 7-day mAR. Staining for primary Abs as indicated and gelatin-DQ (dye-quenched), *i.e.* degraded gelatin. White arrows indicate podosome-rosettes. Scale bar: 3 µm. (**d**) Rapid accumulation of anti-α6 integrin Ab into focal adhesions and podosome rosettes of mAR detected by secondary anti-rat antibody. Immunostaining with primary Abs as indicated. Scale bar: white arrows indicate 10 µm. Podosome-rosettes. (**e**) Quantification of the localization in membrane of anti-α6 integrin Ab. Normalized mean ± SEM of n = 12 regions of interest (ROI), 4 ROI per mAR for a total of 3 mAR per experimental point. (*, P < 0.05 versus *w/o rosette*.) Statistical significance was calculated using unpaired nonparametric Mann-Whitney test. (*right panel*) Schematic representation of the selection of ROIs in panel B. Phalloidin and DAPI stains were used to distinguish the cell edges and phalloidin and cortactin for podosome rosettes. Scale bar: 10 µm. (**f**) Characterization of LifeAct-EGFP mAR endothelial rosettes. Confocal images of immunostainings for primary Abs as indicated. Scale bar: 5 µm. (**g**) Sprout length quantification of capillary-like structures from endothelial α6 null mAR (α_6*fl/fl-Tie2Cre+*.) Normalized mean ± SEM of n = 16 mAR, 4 mAR per mouse from a total of 4 mice. No significative modulation of sprout length was seen. (**h**) Sprout length quantification of capillary-like structures from Laminin α4 KO mAR (*Lama4*$^{-/-}$). Normalized mean ± SEM of n = 8 mAR, 2 mAR per mouse from a total of 4 mice. No significative modulation of sprout length was seen. (**i**) Confocal micrographs of the distribution of immunoreactivity to GoH3 in Riptag2 tumours 10 min after i.v. injection of 25 µg of anti-α6 integrin antibody detected by secondary anti-rat antibody. Immunostaining with primary Abs as indicated. Scale bar: 5 µm. Vessel is delimited by white dotted lines as a guide to the eye; podosome-rosette is indicated by white arrow. (**l**) Confocal micrographs of integrin α6 in podosome rosettes in human tissues. Immunostaining with primary Abs as indicated. Vessel is delimited by white dotted lines as a guide to the eye; podosome-rosettes are indicated by white arrow. Inset, of podosome-rosette. Scale bar: 10 µm.

© 2014 Macmillan Publishers Limited. All rights reserved.

Supplementary video legends

Supplementary Video 1 – Actin dynamics in endothelial podosome rosettes formation. Time-lapse microscopy of LifeAct-RFP localization in EC treated with PMA for the indicated time. Pseudocolors: TIRF in green and EPI in red. EC were seeded on gelatin-coated glass-bottom dishes. Scale bar: 10 μm.

Supplementary Video 2 – Integrin α6 dynamics in adhesive structures during PMA treatment in EC seeded on laminin-rich substrates or not. Time-lapse TIRF microscopy of LifeAct-RFP (red) and α6-GFP (green) localization in EC treated with PMA for the indicated time. EC were seeded on glass-bottom dishes coated with gelatin plus laminin at indicated concentrations. Scale bar: 15 μm.

Supplementary Video 3 – Focal adhesions and podosome rosettes dynamics during PMA treatment. Time-lapse TIRF microscopy of vinculin-RFP (black) localization in EC. EC were cultured in basal medium and then treated with basal medium plus PMA at the indicated time. EC were seeded on gelatin-coated glass-bottom dishes. Scale bar: 20 μm.

Supplementary Video 4 – 3D reconstruction of endothelial podosome rosettes in angiogenic outgrowths. 3D reconstruction of angiogenic outgrowth from mAR into collagen gel. mAR were stimulated with VEGF-A and FGF-2 for 7 days, then fixed and immunostained. Isosurface of F-actin staining was coloured in gray and endothelial rosettes – co-localization of cortactin and F-actin – in red.

Supplementary Video 5 – Endothelial podosome rosettes in angiogenic outgrowth from LifeAct-EGFP mAR. Xyz-section of time-lapse 2-photon microscopy of angiogenic outgrowths from LifeAct-EGFP mAR, stimulated with VEGF-A and FGF-2. In the video the formation of a 5-6 μm-diameter rosette is evident, followed by a cell protrusion of 14-16 μm of length. Top-left panel is the x-plane, top-right is the z-plane, bottom-left is the y-plane and bottom-right is the image. Scale bar: 20 μm.

Supplementary Video 6 – Branching from endothelial rosettes in LifeAct-EGFP mAR. Time-lapse 2-photon microscopy of angiogenic outgrowths from LifeAct-EGFP mAR, stimulated with VEGF-A and FGF-2. Inset, 3D reconstruction of endothelial podosome rosette of the same video. Scale bar: 50 μm.

Supplementary Video 7 – Dynamical analysis of vessel branching in endothelial ITGA6 KO mAR. Time-lapse phase-contrast microscopy of angiogenic outgrowths from mAR. mAR from WT (α6fl/fl-Tie2Cre-) or endothelial α6 KO (α6fl/fl-Tie2Cre+) mice were stimulated with VEGF-A and FGF-2. Scale bar: 70 μm.

Supplementary Video 8 – Dynamical analysis of vessel branching in Lama4$^{-/-}$ KO mAR. Time-lapse phase-contrast microscopy of angiogenic outgrowths from mAR. mAR from *WT* or Laminin α4 null (*LAMA4 mAR*) mice were stimulated with VEGF-A and FGF-2. Scale bar: 70 μm.

Supplementary Video 9 - Dynamical analysis of vessel branching in mAR into laminin-rich matrices. Time-lapse phase-contrast microscopy of angiogenic outgrowths from mAR into type-I-collagen gel with or without 20 μg/ml of laminin addition. mARs were stimulated with VEGF-A and FGF-2. Scale bar: 70 μm.

© 2014 Macmillan Publishers Limited. All rights reserved.